A model of membrane contraction predicting initiation and completion of bacterial cell division

Claire E. Dow,[a,†] Alison Rodger,[*a,b], David I. Roper[c] and Hugo A. van den Berg[d]

Received Xth XXXXXXXXXX 20XX, Accepted Xth XXXXXXXXX 20XX
First published on the web Xth XXXXXXXXXX 200X
DOI: 10.1039/b000000x

Bacterial cell division involves a complex and dynamic sequence of events whereby polymers of the protein FtsZ assemble at the division plane and rearrange to achieve the goal of contracting the cell membrane at the site of cell division, thus dividing the parent cell into two daughter cells. We present a mathematical model (which we refer to as CAM-FF: Critical Accumulation of Membrane-bound FtsZ Fibres) of the assembly of the contractile ring in terms of the accumulation of short linear polymers of FtsZ that associate and dissociate from the cell membrane. In prokaryotes, the biochemical function of FtsZ is thought to underpin the assembly and at least the initial kinetic force of ring contraction. Our model extends earlier work of Surovtsev *et al.* [*PLoS Computational Biology*, 2008, **4**, 7, e1000102] by adding (i) the kinetics of FtsZ accumulation on cell membrane anchor proteins and (ii) the physical forces required to deform the cell against its surface tension. Moreover, we provide a more rigorous treatment of intracellular diffusion and we update some of the model parameters in light of the experimental evidence now available. We derive a critical contraction parameter which links the chemical population dynamics of membrane-bound FtsZ molecules to the force of contraction. Using this parameter as a tool to predict the ability of the cell to initiate division, we are able to predict the division outcome in cells depleted of key FtsZ-binding proteins.

1 Introduction

Co-ordination of cell division, both temporally and spatially, is essential for the propagation of life through successive generations. A key event is the formation of a contractile ring, which is anchored to the cytoplasmic face of the cell membrane at the division plane. Following assembly, the ring contracts, drawing the membrane on opposite sides of the cell together. This divides the parent cell into two daughter cells.[1]

In eukaryotic cells, contraction relies on the sliding force generated by the ATP-dependent interaction of the motor protein myosin and the structural actin filaments within a ring of polymeric actin fibres.[2] As yet no equivalent motor protein has been identified in prokaryotic cells.[3] Whereas in eukaryotes the major structural component is actin, in prokaryotes the ring consists primarily of a tubulin homologue, FtsZ,[4,5] and is referred to as the Z-ring.[6]

Although over two dozen additional proteins have hitherto been found to localise to the division site, evidence suggests that the assembly of the ring and the generation of contractile force are critically dependent on the protein FtsZ.[7] Indeed, purified FtsZ spontaneously forms linear head-to-tail polymers *in vitro*, as well as more complex structures, depending on experimental conditions.[8–11] Moreover, FtsZ is the only component of the division machinery that has homologues in almost all prokaryotic species so far analysed, including the minimal genome of *Mycoplasma genitalium*.[7] This suggests that the presence of FtsZ is a minimum requirement for division to occur. In addition, in *Escherichia coli*, FtsZ-deficient mutants show no indentation of the membrane, whereas mutation of other essential division genes results in some level of indentation even when full division fails.[12] In liposomes seeded with membrane-tethered FtsZ, Z-ring structures are apparent below regions of indented membrane.[13] These results suggest that the force of indentation is generated by FtsZ, at least initially.

Work reported by Surovtsev *et al.*[14] (which we shall refer to as the Surovtsev model) involved analysis of the assembly, maintenance, and contraction of the Z-ring based on kinetic parameters of FtsZ measured *in vitro*. Their model was the first to include the hydrolysis of GTP to GDP and the extension of linear polymers *via* head-to-tail annealing (see Figure 1B(iv)) in addition to polymer elongation by single FtsZ subunits, as used previously by Chen and Erickson[15] in a simpler model of FtsZ polymerisation. The Surovtsev model suggests that the Z-ring consists of long single-stranded FtsZ fila-

[a] *Molecular Organisation and Assembly in Cells Doctoral Training Centre, Coventry House, University of Warwick, Coventry, CV4 7AL, United Kingdom. E-mail: C.E.Dow@warwick.ac.uk*
[b] *Department of Chemistry and Warwick Centre for Analytical Science, University of Warwick, Coventry, CV4 7AL, United Kingdom*
[c] *School of Life Sciences, University of Warwick, Coventry, CV4 7AL, United Kingdom*
[d] *Mathematics Institute, University of Warwick, Coventry, CV4 7AL, United Kingdom*
[†] *The provision of funding by an EPSRC studentship through the MOAC Doctoral Training Centre is gratefully acknowledged*

ments that span the entire circumference of the cell and anneal head-to-tail to form closed polymers. There have been two mechanisms proposed for the contraction of a ring of such a structure: (i) a progressive increase in the lateral overlap of the two ends of the filament forming a spiral structure [16,17] or (ii) that proposed by Surovtsev *et al.* [14]: the progressive loss of FtsZ subunits following GTP hydrolysis with the open ends generated re-annealing.

However, more recent evidence suggests that rather than being composed of long circular polymers, the Z-ring consists of shorter overlapping FtsZ filaments. [3,13] This remains consistent with the "Z-centric" hypothesis: that assembly and the force of constriction originate from FtsZ. In addition, our recent work determined the persistence length of FtsZ (*i.e.* the length over which the polymer naturally remains straight) to be 1.15 ± 0.25 μm. [18] This far exceeds previous estimates and makes it impossible for a single fibre to span the midcell circumference. Accordingly, the central aim of the present paper is to model the assembly of the Z-ring as a collection of shorter, membrane-bound, open filaments in the midcell region. Our model combines a substantial portion of the molecular kinetics developed by Surovtsev *et al.* [14], detailed here in Appendix A, but omits cyclisation as the driving force. We introduce diffusion of FtsZ into the midcell region as well as the interaction of FtsZ with membrane-bound anchor proteins, both additions to the Surovtsev model. Furthermore, we explicitly include the force exerted by FtsZ polymers on the membrane. We also modify some parameters in light of data determined since publication of the Surovtsev model in 2008.

Surovtsev *et al.* [19] have since incorporated their model of Z-ring assembly and contraction into a more complex model of protocell growth and division. They anticipate that the only viable path towards a whole-cell predictive model is *via* the collaborative development of individual modules to be added piecemeal to a global model. We present this work as a development of the Z-ring assembly and contraction module. Lan *et al.* [20] have modelled the deformation and inward growth of the bacterial cell wall originating from the small Z-ring force that deforms the cell with full division dependent on the remodelling of the peptidoglycan layer. We anticipate that this is complementary to our work and forms an additional module of the full cell division model. Our long-term goal is to link the current model with modules for: (i) the membrane bending, (ii) the link to the outer membrane remodelling, and (iii) the outer membrane remodelling.

§2 introduces the equations describing the dynamics of FtsZ polymerisation, much of which follows the work of Surovtsev *et al.* [14], and the concentration of FtsZ at the midcell membrane. §2 concludes with our new analysis of the force required for Z-ring contraction, leading to the definition of a key quantity which we call the *contraction parameter*. §3 shows that by implementing the wild-type parameter values, estimated from the current experimental literature, the model solutions are in accordance with the properties of the Z-ring measured *in vivo*. In §4 we show that the contraction parameter is a useful tool to predict the division outcome in cells, such as on depletion of the membrane-anchor proteins. §5 contains an analysis of the model assumptions.

2 Model

In the nascent daughter cell, FtsZ monomers are dispersed throughout the cytosol. [21] Formation of the Z-ring for the next cell division therefore requires polymerisation of FtsZ, polymer localisation at the midcell and polymer anchoring to the cell membrane. In the present model, which we refer to as CAM-FF: Critical Accumulation of Membrane-bound FtsZ Fibres, the cell is conceptually divided into three compartments: the midcell region, the adjoining cell caps, and the midcell membrane, as shown in Figure 1A. All FtsZ molecules are initially monomeric and dispersed within the cell caps and midcell compartments. A system of ordinary differential equations (ODEs) describes the changes in the concentrations of FtsZ molecules within the three compartments over time, as detailed in Appendix B. FtsZ molecules within the cell caps and the midcell region undergo the polymerisation and GTP hydrolysis reactions as shown in Figure 1B. Movement between these two compartments is by diffusion. Movement occurs from the midcell region to the midcell membrane when FtsZ molecules bind to anchor sites fixed to the membrane and *via* polymerisation reactions between membrane-bound FtsZ and free (unbound) FtsZ in the midcell region. The model explicitly accommodates the interaction of single FtsZ polymers with multiple membrane anchor sites as depicted in Figure 1C. Once bound to the membrane, the length of the polymer may increase by the addition of unbound FtsZ monomers and polymers but we assume that polymerisation reactions do not occur between membrane-bound FtsZ molecules due to the low density of anchor molecules on the membrane surface. There is evidence of some polymerisation on the surface in the data from Mateos-Gil *et al.* [22] but this is at 40 times the density of the *in vivo* situation. GTP hydrolysis and polymer dissociation are assumed to occur within membrane-bound polymers in the same way as for free polymers. We do not include the lateral interaction of FtsZ polymers since, according to Erickson [23], when the subunit entropy contribution is considered, a contraction mechanism based on FtsZ polymer sliding is implausible. Thus the FtsZ:FtsZ lateral interactions are not the key to membrane contraction.

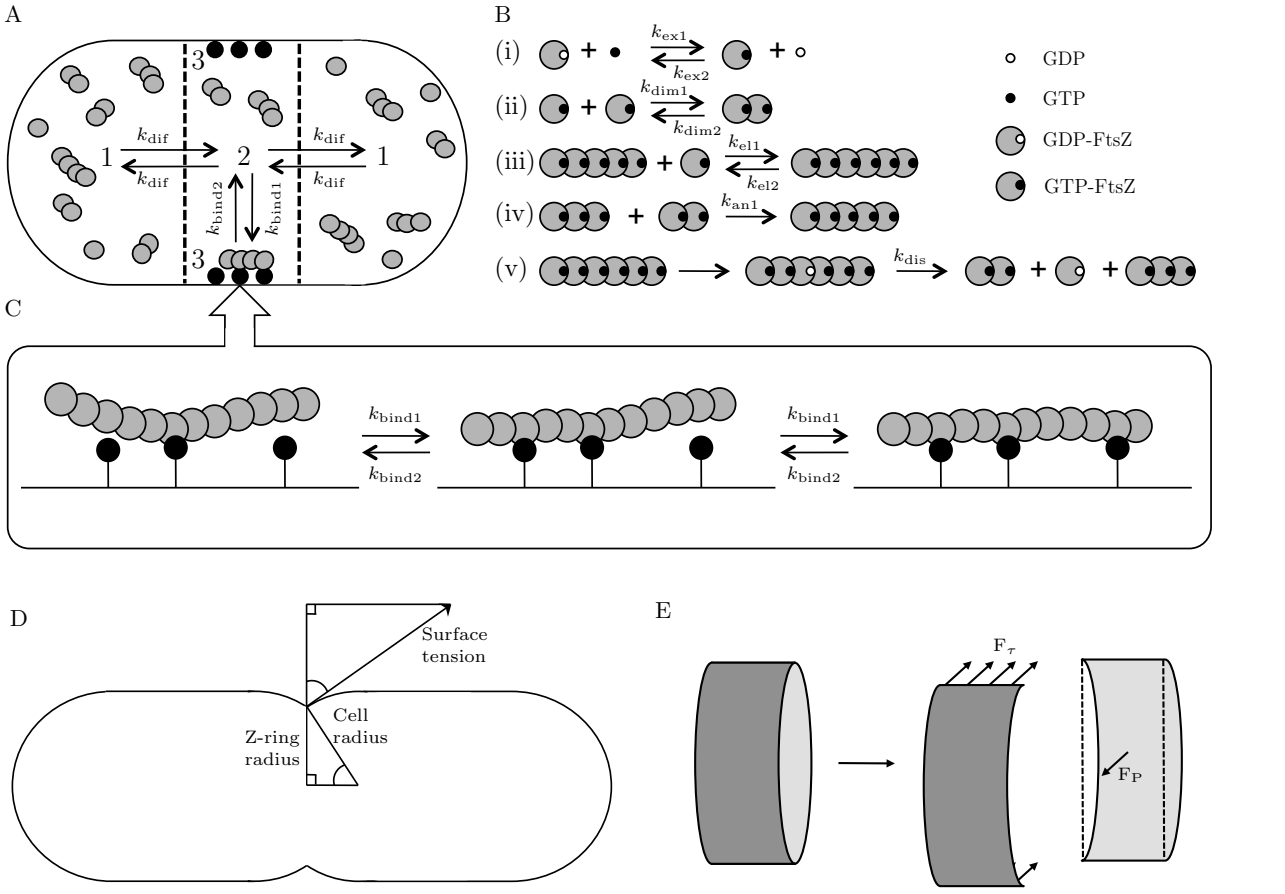

Fig. 1 Schematic diagram of the cell model used in this work. (A) The cell is conceptually divided into three compartments: the cell caps (1), the midcell (2), and the midcell membrane (3). FtsZ moves between the cell caps and the midcell regions by diffusion. Exchange between the midcell region and the midcell membrane is *via* the interaction of FtsZ with membrane anchor sites and subsequent polymerisation. (B) Using the notation of Surovtsev *et al.* [14], the chemical reactions in our model are: nucleotide exchange (i), dimerisation (ii), and elongation (iii) (reversible processes) and annealing (iv) (assumed to be irreversible in the absence of GTP hydrolysis) and polymer breakdown following GTP hydrolysis (v) (also irreversible). (C) Depending on the anchor density, an FtsZ polymer may bind to multiple anchor sites. As polymer length increases, the number of anchor connections increases thereby lowering the probability that the polymer will be released from the membrane. (D) Z-ring contraction pulls the membrane inwards against the outward force from the cell surface tension. (E) For the slice through the Z-ring, at equilibrium the horizontal force due to the ring tension (F_τ) is balanced by the internal pressure acting over the cross-sectional area of the slice (F_P).

2.1 FtsZ polymerisation and GTP hydrolysis: the Surovtsev model rewritten

The molecular kinetics of FtsZ polymerisation and GTP hydrolysis/dissociation summarised in Equations (1) to (6) are the rate equations as proposed by Surovtsev *et al.* [14]. FtsZ is a GTP/GDP-binding protein that interconverts GTP and GDP.[24] The nucleotide-binding site is exposed to the cytosol allowing for a bound nucleotide to be released, leaving the site open for another nucleotide to bind in nucleotide exchange. The relative concentrations of GTP-bound and GDP-bound FtsZ monomers therefore depend on the relative concentrations of GTP and GDP in the cytosol. In CAM-FF, all FtsZ monomers are initially GDP-bound reflecting the starting point for some *in vitro* experiments[25] and the depolymerisation of the Z-ring in the previous cell division event.[21] The rates of nucleotide exchange for monomeric FtsZ in solution are given by

$$R_{\mathrm{ex1}} = k_{\mathrm{ex1}}\,[\mathrm{GTP}]\,Z_{\mathrm{D}} \quad \text{and} \quad R_{\mathrm{ex2}} = k_{\mathrm{ex2}}\,[\mathrm{GDP}]\,Z_{\mathrm{T}}\,, \qquad (1)$$

where Z_{D} and Z_{T} are the concentrations of GDP-bound and GTP-bound FtsZ monomers, respectively. In the GTP-bound state, FtsZ molecules polymerise rapidly *in vitro* forming head-to-tail subunit chains.[10] In CAM-FF, the rates of dimerisation and elongation of GTP-bound FtsZ are given by forward and reverse rates,

$$R_{\mathrm{dim1}} = k_{\mathrm{dim1}}\,Z_{\mathrm{T}}^2\,, \quad R_{\mathrm{dim2}} = k_{\mathrm{dim2}}\,Z_2 \qquad (2)$$

and

$$R^i_{\mathrm{el1}} = k_{\mathrm{el1}} Z_{\mathrm{T}} Z_i \,, \quad R^i_{\mathrm{el2}} = k_{\mathrm{el2}} Z_{i+1} \,, \tag{3}$$

respectively, where Z_2 is the concentration of FtsZ dimers and Z_i is the concentration of FtsZ polymers of length i subunits. We assume the rate of elongation does not depend on the length i. The rates of dimerisation and elongation of GDP-bound FtsZ are assumed to be zero.[10] We assume the forward rates of dimerisation and elongation to be equal; for the corresponding dissociation, the rate constant has been found to be higher for the dissociation of FtsZ dimers than for the dissociation of FtsZ polymers.[26] This is reflected in the values of the rate constants k_{dim2} and k_{el2}, see §3.

Polymer length can also increase by annealing reactions, in which a polymer of length i is formed by the annealing of a polymer of length j to a polymer of length $i-j$. This occurs with rate

$$R^i_{\mathrm{an1}} = k_{\mathrm{an}} \sum_{j=2}^{i-2} \frac{1+\delta_{j\,i-j}}{2} Z_j Z_{i-j} \,, \tag{4}$$

and the removal of polymers due to annealing is given by

$$R^i_{\mathrm{an2}} = k_{\mathrm{an}} Z_i \sum_{j=2}^{i_{\max}-i} (1+\delta_{i\,j}) Z_j \,, \tag{5}$$

where $i_{\max}$ is the maximum length polymer that can form in the model. In principle, the model should allow for arbitrarily long filaments, *i.e.* $i_{\max} \to \infty$, but for the purpose of calculation a cut-off value is selected that is sufficiently large such that the results do not depend on the value chosen. We do not include reverse rates for the annealing reaction since we assume that depolymerisation does not occur in the absence of GTP hydrolysis.

On polymerisation, a GTPase active site is formed when a catalytic aspartate residue of one subunit inserts into the GTP-binding pocket of the adjacent subunit.[27,28] Once polymerised, the nucleotide state of an FtsZ subunit may therefore switch from GTP-bound to GDP-bound. *In vitro*, depletion of GTP leads to net depolymerisation, which suggests that the GDP-bound polymers are unstable.[10] Surovtsev *et al.*[14] assumed that upon GTP hydrolysis, the GDP-bound subunit dissociates from the intact polymers on either side instantaneously. We use the equivalent rate equation given by

$$R^i_{\mathrm{dis}} = (i-1)\, k_{\mathrm{dis}} Z_i \,, \tag{6}$$

where a polymer of length i has $i-1$ GTPase active sites. However, instead of the hydrolysis rate of 0.15 s^{-1} as used by Surovtsev *et al.*[14], to account for the rate of dissociation of FtsZ following hydrolysis, we use the value of k_{cat} from Romberg and Mitchison[25] of 4.5 min^{-1} per FtsZ to give rate constant $k_{\mathrm{dis}} = 0.075$ s^{-1}. The rate constant k_{dis} is equal for all GTPase active sites since it has been shown that all monomer interfaces are equally competent for hydrolysis.[22] The significance of the change in the model is that we now account for the time spent by FtsZ subunits within polymers in the GDP-bound state following hydrolysis, prior to dissociation.

2.2 Novel features of our membrane contraction model

2.2.1 FtsZ diffusion. In CAM-FF, we consider the change in the midcell concentration due to diffusion from the cell caps to the midcell for FtsZ molecules of length i to be given by

$$R^i_{\mathrm{cm}} = k_{\mathrm{dif}} (Z^{\mathrm{cc}}_i - Z^{\mathrm{mid}}_i)/V_{\mathrm{mid}} \,, \tag{7}$$

and that for the diffusion from the midcell to the cell caps to be

$$R^i_{\mathrm{mc}} = k_{\mathrm{dif}} (Z^{\mathrm{mid}}_i - Z^{\mathrm{cc}}_i)/V_{\mathrm{cc}} \,, \tag{8}$$

where k_{dif} is the diffusion constant, which is assumed to be equal for all values of i, and V_{cc} and V_{mid} are the volumes of the cell caps and midcell compartments, respectively. The rate of diffusion defined in Equations (7) and (8) applies to all polymer lengths and for both GDP- and GTP-bound FtsZ monomers.

The process of diffusion without any other factor will ensure a uniform concentration of FtsZ throughout the cell. To model the accumulation of FtsZ at the midcell and the physical attachment that confers a pinching force, we introduce to our model a compartment corresponding to the midcell membrane.

2.2.2 Membrane binding: Interaction of FtsZ polymers with multiple binding sites. To anchor to the cell membrane *in vivo*, FtsZ interacts directly with the membrane-binding proteins proteins ZipA and FtsA.[29] The anchoring means that if the Z-ring constricts, it exerts a pinching force on the cell membrane.

The rate of attachment of the FtsZ polymers within the midcell compartment is given by

$$R^i_{\mathrm{bind1}} = i\, k_{\mathrm{bind1}} Z^{\mathrm{mid}}_i \left(\frac{10^{21} B}{N_{\mathrm{A}} V_{\mathrm{bnd}}} - \left(Z^{\mathrm{bnd}}_{\mathrm{D}} + Z^{\mathrm{bnd}}_{\mathrm{T}} + \sum_{j=2}^{i_{\max}} S(j) Z^{\mathrm{bnd}}_j \right) \right) \,, \tag{9}$$

for $i \geq 2$, where B is the total number of binding sites, V_{bnd} is the volume of the midcell membrane compartment, N_{A} is Avogadro's number and $S(j)$ is the expected number of binding sites occupied by a polymer of length j. Multiplication by i reflects the number of potential anchor binding sites along an FtsZ polymer of length i. GDP- and GTP-bound monomers

may bind to the midcell membrane with rates given by

$$R^{\mathrm{D}}_{\mathrm{bind1}} = k_{\mathrm{bind1}}\, Z^{\mathrm{mid}}_{\mathrm{D}} \left(\frac{10^{21} B}{N_{\mathrm{A}} V_{\mathrm{bnd}}} - \left(Z^{\mathrm{bnd}}_{\mathrm{D}} + Z^{\mathrm{bnd}}_{\mathrm{T}} + \sum_{j=2}^{i_{\max}} S(j)\, Z^{\mathrm{bnd}}_{j} \right) \right) \tag{10}$$

and

$$R^{\mathrm{T}}_{\mathrm{bind1}} = k_{\mathrm{bind1}}\, Z^{\mathrm{mid}}_{\mathrm{T}} \left(\frac{10^{21} B}{N_{\mathrm{A}} V_{\mathrm{bnd}}} - \left(Z^{\mathrm{bnd}}_{\mathrm{D}} + Z^{\mathrm{bnd}}_{\mathrm{T}} + \sum_{j=2}^{i_{\max}} S(j)\, Z^{\mathrm{bnd}}_{j} \right) \right) , \tag{11}$$

respectively. Release from the membrane is given by

$$R^{i}_{\mathrm{bind2}} = k_{\mathrm{bind2}}\, p_1(i)\, Z^{\mathrm{bnd}}_{i} \quad \text{for } i \geq 2 , \tag{12}$$

where $p_1(i)$ is the fraction of polymers of length i expected to be attached to the membrane by a single binding site only. For GDP- and GTP-bound monomers, the rates of release are given by

$$R^{\mathrm{D}}_{\mathrm{bind2}} = k_{\mathrm{bind2}}\, Z^{\mathrm{bnd}}_{\mathrm{D}} \quad \text{and} \quad R^{\mathrm{T}}_{\mathrm{bind2}} = k_{\mathrm{bind2}}\, Z^{\mathrm{bnd}}_{\mathrm{T}} , \tag{13}$$

respectively. On release, polymers return to the midcell soluble population.

To determine $p_1(i)$, the binding of polymers to multiple binding sites is modelled as a Markov chain with a fixed number of binding sites available. We assume that the anchor proteins interact with single FtsZ subunits allowing a polymer of length i subunits to potentially form i membrane interactions.

At equilibrium, the fraction of polymers bound to a single binding site is given by

$$f^{j}_{1} = \frac{j}{\kappa(1+\frac{1}{\kappa})^{j} - \kappa} , \tag{14}$$

where j is the number of binding sites available and κ is the dissociation constant. A full derivation of Equation (14) is given in Appendix C. Since each anchor interacts with a single FtsZ subunit within the polymer, the probability that j binding sites are available to a polymer of length i is given by

$$\mathrm{P}(j \text{ sites}) = \binom{i}{j} \frac{\mathrm{P}_a^{j} (1-\mathrm{P}_a)^{i-j}}{1-(1-\mathrm{P}_a)^{i}} , \tag{15}$$

where P_a is the probability that one FtsZ subunit is adjacent to a binding site. This equation is derived by conditioning the binomial distribution on at least one binding site being available, since for a molecule in the membrane-bound fraction, this condition is satisfied. The fraction expected to be attached by a single anchor is the expectation of fractions for all values of j from 1 to i:

$$p_1(i) = \sum_{j=1}^{i} \binom{i}{j} \frac{\mathrm{P}_a^{j} (1-\mathrm{P}_a)^{i-j}}{1-(1-\mathrm{P}_a)^{i}} \cdot \frac{j}{\kappa(1+\frac{1}{\kappa})^{j} - \kappa} . \tag{16}$$

Since a polymer is held on the membrane until the final FtsZ-anchor interaction is broken, adjustment of the rate of release using the fraction of polymers in the singly-bound state accounts for the binding to multiple sites.

The binding rate is proportional to the number of available binding sites. The available number depends on the total number of binding sites and the number of occupied binding sites, which itself depends on the membrane-bound FtsZ population. The expected number of sites occupied by a chain of length i is given by

$$S(i) = \frac{\mathrm{P}_a\, i}{1-(1-\mathrm{P}_a)^{i}} , \tag{17}$$

which is again conditional on at least one site being occupied by a membrane-bound polymer.

2.2.3 Polymerisation of membrane-bound FtsZ. For membrane-bound monomeric FtsZ, we assume that nucleotide exchange occurs as for soluble FtsZ, *cf.* Equation (1). The extension of membrane-bound FtsZ polymers occurs by interaction with unbound, soluble FtsZ in the midcell region. By analogy to Equations (2) and (3) for soluble FtsZ, the rates of dimerisation and elongation of membrane-bound FtsZ are given by

$$R_{\mathrm{dim1\_bnd}} = k_{\mathrm{dim1}}\, Z^{\mathrm{mid}}_{\mathrm{T}}\, Z^{\mathrm{bnd}}_{\mathrm{T}} , \quad R_{\mathrm{dim2\_bnd}} = k_{\mathrm{dim2}}\, Z^{\mathrm{bnd}}_{2} \tag{18}$$

and

$$R^{i}_{\mathrm{el1\_bnd}} = k_{\mathrm{el1}}\, Z^{\mathrm{mid}}_{\mathrm{T}}\, Z^{\mathrm{bnd}}_{i} , \quad R^{i}_{\mathrm{el2\_bnd}} = k_{\mathrm{el2}}\, Z^{\mathrm{bnd}}_{i+1} , \tag{19}$$

respectively. For the reverse reactions, it is assumed that a GTP-bound FtsZ monomer returns to the midcell region while the shortened polymer (which is a GTP-bound monomer in the case of the reverse of dimerisation) remains bound to the midcell membrane. The rate of polymer annealing is given by

$$R^{i}_{\mathrm{an1\_bnd}} = k_{\mathrm{an}} \sum_{j=2}^{i-2} Z^{\mathrm{bnd}}_{j}\, Z^{\mathrm{mid}}_{i-j} , \tag{20}$$

with the removal of polymers due to annealing given by

$$R^{i}_{\mathrm{an2\_bnd}} = k_{\mathrm{an}}\, Z^{\mathrm{mid}}_{i} \sum_{j=2}^{i_{\max}-i} Z^{\mathrm{bnd}}_{j} , \tag{21}$$

and

$$R^{i}_{\mathrm{an2\_mid}} = k_{\mathrm{an}}\, Z^{\mathrm{bnd}}_{i} \sum_{j=2}^{i_{\max}-i} Z^{\mathrm{mid}}_{j} , \tag{22}$$

for the midcell region and midcell membrane, respectively. The Kronecker delta used in Equations (4) and (5) for the annealing reactions of soluble FtsZ is not required since the double-counted combinations for the soluble case are no longer equivalent in the case of interaction of a membrane-bound population with a soluble population. As for soluble FtsZ, the annealing reactions are assumed to be irreversible. The value of rate constants for dimerisation, elongation, and annealing are assumed in the model to be equal to those for reactions between soluble FtsZ.

2.2.4 Hydrolysis of membrane-bound polymers. The GDP-bound subunit and the shorter polymer(s), generated by the polymer cleavage that follows a hydrolysis/dissociation event, may remain bound to the membrane or may return to the soluble midcell compartment, depending on their attachment to adjacent binding sites. For a parent polymer of length i', the probability that any subunit is adjacent to a binding site is given by

$$\mathrm{P}(\text{site adjacent} \mid i') = \frac{\mathrm{P}_a}{1-(1-\mathrm{P}_a)^{i'}} \,. \tag{23}$$

Therefore, for a polymer of length i, formed as a result of a hydrolysis/dissociation reaction, the probability that the polymer returns to the midcell compartment is the probability that none of the i subunits is adjacent to a binding site which is given by

$$\mathrm{P}_i(\text{no sites} \mid i') = \left(1-\frac{\mathrm{P}_a}{1-(1-\mathrm{P}_a)^{i'}}\right)^{i} \,. \tag{24}$$

The probability that a polymer remains in the membrane-bound fraction is therefore $1-\mathrm{P}_i(\text{no sites} \mid i')$. It is assumed that the fraction of those with at least one adjacent binding site will join the population of membrane-bound polymers of length i. The interaction of FtsZ with FtsA or ZipA does not affect the rate of GTP hydrolysis *in vitro*.[30,31] Therefore, the rate of dissociation of membrane-bound polymers remains as given by Equation (6) for soluble FtsZ in § 2.1.

We do not directly account for the potential of membrane-bound polymers to reanneal after fragmentation. However, the increased likelihood that a GTP hydrolysis/dissociation event occurring towards either end of the FtsZ polymer results in permanent loss of subunits from the polymer, compared to a GTP hydrolysis/dissociation event in the centre of the polymer, as found by Mateos-Gil *et al.*[22], is accounted for in the model. By calculation of the number of binding sites available to the polymer fragments produced on dissociation, smaller polymers are less likely to be bound to an anchor and so are more likely to move back to the soluble fraction with loss from the Z-ring. Although fragments that remain bound do not reanneal, they are available for reannealing to free (unbound) FtsZ polymers and remain within the Z-ring compartment.

2.2.5 Tension in the Z-ring. Two key properties govern Z-ring contraction. The first is the total tension of the Z-ring, τ_Z, defined in terms of the cell surface tension and the radius of the Z-ring as contraction proceeds. The second is the maximum tension the Z-ring can withstand, $\hat{\tau}$, at a given radius, ς, based on the population of FtsZ polymers assembled and the force of the interaction between FtsZ and the membrane anchor. The analysis shown in Appendix D, in which the components of the cell surface tension and the forces acting on the Z-ring are considered as in Figure 1D and Figure 1E respectively, shows that τ_Z, the total tension of the Z-ring during contraction, is given by

$$\tau_\mathrm{Z} = \tau_0 \left(1+\frac{2r}{\omega}\rho\sqrt{1-\rho^2}\right) \,, \tag{25}$$

where τ_0 is the cell surface tension, ω is the width of the Z-ring, and $\rho = \varsigma/r$ is the dimensionless ratio of the radius of the Z-ring during contraction, ς, to the radius of the Z-ring before contraction, r. For the sake of simplicity, the parameters τ_0 and ω are assumed to be constant throughout the contraction process.

As shown in Appendix D, the maximum tension the Z-ring can withstand $\hat{\tau}$ is given by

$$\hat{\tau} = F\,\frac{\mathrm{P}_a l_0}{\omega r}\,.\,\frac{\bar{i}^2 N_\mathrm{Z}}{\rho} \,, \tag{26}$$

where F is proportional to the force of the interaction of FtsZ with a single anchor site, l_0 is the length of one FtsZ subunit, $\bar{i}$ is the average number of subunits per polymer, and N_Z is the total number of polymers bound to the membrane.

In the model, the sign of $\frac{\mathrm{d}}{\mathrm{d}t}(\varsigma)$ agrees with that of $(\tau_\mathrm{Z}-\hat{\tau})$ because it is assumed that this difference will drive the contraction. The precise functional form of the relationship depends on the molecular mechanism of contraction, which remains to be elucidated. In the absence of detailed data, a simple linear relationship is proposed:

$$\frac{\mathrm{d}}{\mathrm{d}t}\varsigma = \vartheta_0\,(\tau_\mathrm{Z}-\hat{\tau}) \,, \tag{27}$$

where ϑ_0 is a constant. Substituting the total ring tension and maximum sustainable tension, defined in Equations (25) and (26) respectively, gives an ODE for the rate of change of the dimensionless ratio ρ, the size of the ring relative to its starting size:

$$\frac{\mathrm{d}}{\mathrm{d}t}\rho = \vartheta\left(\alpha\left(1+\gamma\rho\sqrt{1-\rho^2}\right)-\frac{\bar{i}^2 N_\mathrm{Z}}{\rho}\right) \,, \tag{28}$$

where

$$\vartheta \triangleq \frac{\vartheta_0 F \mathrm{P}_a l_0}{\omega r} \,, \quad \alpha \triangleq \frac{\tau_0 \omega r}{F \mathrm{P}_a l_0} \,, \quad \text{and} \quad \gamma \triangleq \frac{2r}{\omega} \,. \tag{29}$$

Hidden in these parameters are the details of membrane bending energy and the molecular reorganisation that occurs concomitantly with the contraction. A full model of bacterial cell division would complement CAM-FF with a membrane remodelling module. Contraction corresponds to the rate of change of ρ being negative. Therefore, contraction proceeds if and only if

$$\bar{i}^2 N_Z > \alpha\rho\,(1+\gamma\rho\sqrt{1-\rho^2})\,. \tag{30}$$

The ability of the cell to divide thus depends on the value of the *contraction parameter*:

$$\chi \triangleq \bar{i}^2 N_Z\,. \tag{31}$$

Initially, $\rho = 1$ and contraction therefore begins when $\chi > \alpha$. Numerical solution of the system of ODEs, given in full in Appendix B, allows determination of χ under various biological scenarios and prediction of the ability of cells to initiate and sustain division (since Equation (30) also tells us if contraction stops).

Since the average length of polymers $\bar{i}$ is squared in the calculation of the contraction parameter, for a given number of FtsZ subunits bound to the membrane, a smaller number of longer polymers are expected to collectively provide a stronger contractile force than a larger number of shorter polymers.

3 Estimation of wild-type rate constants

Surovtsev *et al.*[14] selected rate constants based on the best available experimental data. However, we use a lower value of $[\text{FtsZ}]_{\text{Total}}$. Based on the 15,000 molecules of FtsZ per cell found by Lu *et al.*[32], $[\text{FtsZ}]_{\text{Total}} = 12\ \mu$M. Although lower values for the number of FtsZ molecules have been found[33,34], we use the highest of the recorded numbers since we use a large volume to calculate the corresponding concentration. Whereas, the effective volume available to the FtsZ will be much lower??? - I don't know how to word this! We retain the values used by Surovtsev *et al.*[14] for [GTP], [GDP] and $i_{\max}$. The value of $i_{\max} = 150$ subunits is consistent with the average length of FtsZ polymers measured *in vitro* using transmission electron microscopy of 23 subunits[35] and we have ensured that this is sufficiently large that the results are independent of its value. An increase in the value to $i_{\max} = 200$ does not change the predicted average lengths of free and membrane-bound FtsZ polymers, the predicted number of membrane-bound FtsZ molecules nor the predicted percentage of FtsZ incorporation into the Z-ring. We also follow Surovtsev *et al.*[14] in representing the cell as a cylinder with radius 0.4 μm, length 4 μm, and midcell region width 0.1 μm. In contrast to them, we include the whole midcell slice, as shown in Figure 2, not just a region of depth 8 nm. The volumes of the cell caps and midcell regions are therefore $V_{\text{cc}} = 2.0\ \mu\text{m}^3$ and $V_{\text{mid}} = 0.05\ \mu\text{m}^3$ respectively. For the midcell radius of 0.4 μm and the midcell width of 0.1 μm, this corresponds to a midcell membrane surface area of 0.25 μm^2. The depth of the midcell membrane was set to 4 nm (the size of an FtsZ subunit) giving a volume $V_{\text{bnd}} = 1.0\times10^{-3}\ \mu\text{m}^3$. As the diffusion constant D of ovalbumin, which is of similar size to FtsZ, is 78 $\mu\text{m}^2\text{s}^{-1}$,[36] we use this value for the diffusion constant of FtsZ. Fick's Law gives the flux across the diffusion area A equal to $\frac{AD}{L}\Delta C$ where ΔC is the concentration difference between the two compartments and L is the distance between the midpoint of the two compartments, in this case 1 μm. In our model, the flux in equivalent units is given by $k_{\text{dif}}(Z_i^{\text{cc}} - Z_i^{\text{mid}})$, Equation (7), whence $k_{\text{dif}}\Delta C = \frac{AD}{L}\Delta C$. Therefore, $k_{\text{dif}} = \frac{AD}{L}$. The value for the diffusion area A is given by the bounding area of the midcell slice, $2\pi r^2$, see Figure 2, giving $k_{\text{dif}} \approx 78\ \mu\text{m}^3\text{s}^{-1}$. This is equal to the original value of the diffusion constant D since the diffusion distance is taken as 1 μm and the area of the boundaries of the slice are approximately equal to 1 μm^2 for a radius of 0.4 μm.

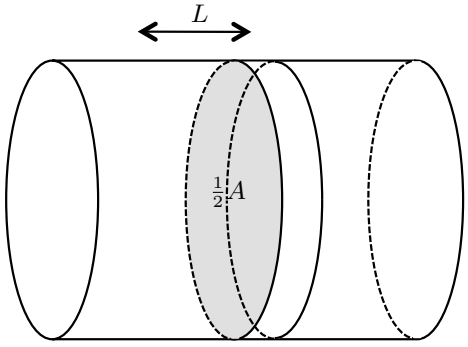

Fig. 2 The rate constant for the diffusion of FtsZ from the cell caps into the midcell region, k_{dif}, is estimated using Fick's Law assuming diffusion through area A along a path of length L.

A key parameter in our model is the fraction of membrane-bound FtsZ polymers which are in the singly-bound state. This depends on the probability that a subunit is adjacent to a binding site, P_a, and on the dissociation constant κ. We assume the two anchor interactions (ZipA and FtsA) have the same binding strength. The FtsEX complex may provide an additional anchoring role since FtsX is an intergral membrane protein and is linked to FtsZ via the soluble protein FtsE.[37,38] However, the role of FtsEX in cell division is unclear and key data are missing such as the number of molecules per cell. The anchoring role of FtsEX has, for now, been omitted. The experimental literature cites the number of molecules per cell for ZipA and FtsA as 1500 and 740, respectively[33] and using fluorescent-labelled ZipA, Stricker *et al.*[39] found that approximately 30% of the cell complement of ZipA localises to the

Z-ring *in vivo*. Therefore, it is assumed that 30% of the cell complement of anchors are found in the midcell membrane compartment. By dividing the surface area of the membrane into a grid of squares 4 nm × 4 nm, P_a is given by the proportion of grid squares occupied by 30% of the total number of anchor proteins. This gives $P_a = 0.043$. The wild-type dissociation constant of 0.2 μM for the FtsZ-ZipA (and hence the other) interactions was used to give κ.[40] Figure 3 shows $p_1(i)$, the fraction of polymers expected to be attached to the membrane by a single binding site only, for $P_a = 0.043$ and $\kappa = 0.2$ μM. The high proportion of polymers that remain in the singly-bound state for shorter lengths reflects the observation that although an FtsZ polymer of length i has the potential to form i FtsZ:anchor interactions, ZipA interacts with FtsZ substoichiometrically.[41] The interaction data presented by Martos *et al.*[41] shows that oligomers of FtsZ, up to hexamers, bind to a single ZipA molecule. This is reflected in the model as the predicted number of anchor proteins occupied by FtsZ oligomers at the membrane is 1 for an FtsZ monomer, up to 1.11 for a hexamer.

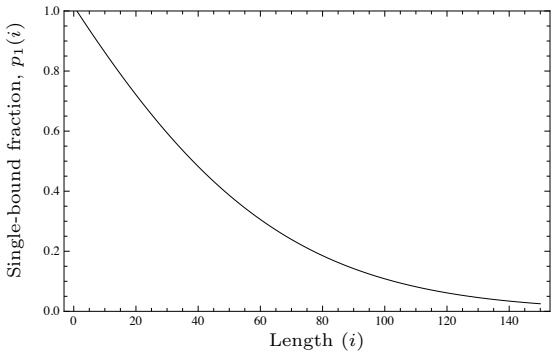

Fig. 3 The fraction of membrane-bound polymers expected to be attached by a single FtsZ-anchor interaction, as a function of polymer length for $P_a = 0.043$ and $\kappa = 0.2$ μM.

Fluorescence recovery after photobleaching (FRAP) experiments have shown the half life of recovery of fluorescence in the Z-ring for wild-type FtsZ in *E. coli* to be 30 sec.[39] Since the recovery of fluorescence in the bleached patch of the Z-ring is exponential, the observed rate of recovery is given by $\ln 2/t_{1/2}$. For a half life of recovery of 30 seconds, the corresponding observed rate of release from the membrane is 0.023 s^{-1}. Since the steady state of Z-ring assembly has been reached prior to the photobleaching, it follows that $k_{\text{bind2}} p_1(\bar{i})$ (see Equations (12) and (16)) equals 0.023 s^{-1} (where $\bar{i}$ is the average membrane-bound polymer length at equilibrium). With the dissociation constant κ fixed at 0.2 μM, it follows that the lower bounds of k_{bind1} and k_{bind2} are 0.142 $\mu M^{-1}s^{-1}$ and 0.0284 s^{-1}, respectively.

For the wild-type parameter values as shown in Table 1,

Table 1 Wild-type parameter values

Parameter	Wild-type value	Units	Reference
$[\text{FtsZ}]_{\text{Total}}$	20	μM	14
[GTP]	90	μM	14
[GDP]	10	μM	14
B	672	-	33
P_a	0.043	-	14,33
κ	0.2	μM	40
$i_{\max}$	150	-	14
k_{ex1}	0.01	$\mu M^{-1}s^{-1}$	14,26,42
k_{ex2}	0.005	$\mu M^{-1}s^{-1}$	14,26,42
k_{dim1}	4	$\mu M^{-1}s^{-1}$	14,26
k_{dim2}	40	s^{-1}	14,26
k_{el1}	4	$\mu M^{-1}s^{-1}$	14,26
k_{el2}	0.4	s^{-1}	14,26
k_{an}	4	$\mu M^{-1}s^{-1}$	14,26
k_{dis}	0.15	s^{-1}	25
k_{dif}	78	$\mu m^3 s^{-1}$	36
k_{bind1}	0.142	$\mu M^{-1}s^{-1}$	39,40
k_{bind2}	0.0284	s^{-1}	39,40

the NDSolve function of Wolfram *Mathematica* 8 was used to numerically solve the ODEs as provided in Appendix B. As described in Appendix E, including both the diffusion of FtsZ into the midcell region in a more physically realistic manner and an explicit model of membrane binding, prevents the truncation artefact arising in the Surovtsev model where long polymers accumulate thus increasing the concentrations of large polymers up to $i_{\max}$. CAM-FF predicts that the average FtsZ polymer length for the membrane-bound population is 14 subunits, which is considerably lower than in the Surovtsev model.[14] The average membrane-bound FtsZ polymer length of 14 subunits for the total of 504 polymers membrane-bound at equilibrium, gives a total polymer length of 29.3 μm. This is sufficient to span the circumference over 11 times. This overlap of short FtsZ filaments on the membrane is consistent with the hypothesis that Z-ring formation proceeds by overlap of short FtsZ polymers.[13] In the wild-type, our model predicts that the average polymer length at equilibrium for soluble FtsZ is 4 subunits in both the cell caps and midcell regions.

In the Surovtsev model, 80% of the cell complement of FtsZ was found at the midcell due to the enforced confinement to this region.[14] In CAM-FF, the percentage incorporation of FtsZ into the membrane-bound Z-ring is predicted to be 28%, in accordance with the value measured experimentally of 30–35%.[39,43]

Figure 4 shows the value of the contraction parameter χ over time for the wild type. The contraction parameter in-

creases reaching its maximum value on formation of the Z-ring.

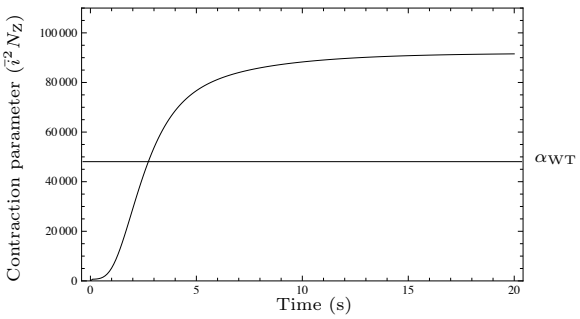

Fig. 4 The contraction parameter χ increases to a maximum value on formation of the Z-ring. Parameter values as shown in Table 1.

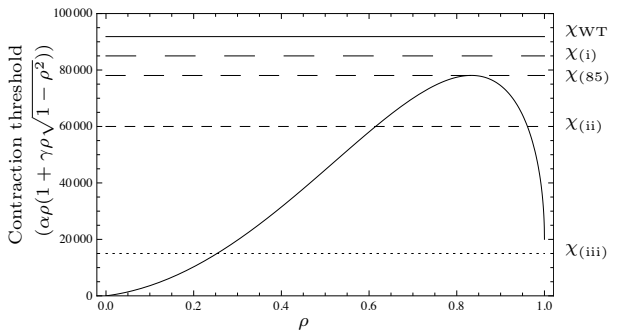

Fig. 5 The contraction threshold value varies as the radius of the Z-ring decreases. Using the wild-type value of the contraction parameter χ_{WT} and the 85% tolerance limit χ_{85}, for the parameter values in Table 1, $\alpha = 20,000$. $\gamma = 8$. Since the contraction parameter χ must exceed the contraction threshold at all values of the radius ratio from 1 to 0 for contraction to proceed, the model predicts three division outcomes: $\chi_{(i)}$ division proceeds to completion, $\chi_{(ii)}$ division is initiated but stalls prior to completion and $\chi_{(iii)}$division is not initiated.

4 The contraction parameter predicts division outcome

The key parameter in CAM-FF is the contraction parameter χ which is a useful tool to predict the ability of cells to initiate and continue Z-ring contraction. Once contraction is initiated, the evolution of both the contraction parameter and the contraction threshold determine whether Z-ring constriction proceeds to completion. For the Z-ring radius to continue to decrease, χ must remain greater than $\alpha\rho\,(1+\gamma\rho\sqrt{1-\rho^2})$. If the width of the Z-ring is assumed to be constant during contraction, γ is constant at 8 (*cf.* Equation (29)) and the contraction threshold is a function of ρ, the dimensionless ratio of the radius of the Z-ring at time t to the initial radius. The plot of χ vs ρ is given in Figure 5 for the wild-type case. CAM-FF predicts three possible division outcomes: (i) division proceeds to completion, (ii) division is initiated but stalls prior to completion and (iii) division is not initiated. These scenarios are highlighted in Figure 5, on the assumption that the contraction parameter χ remains constant throughout the division process. The value of the initiation threshold α is currently unknown. Therefore, using the wild-type parameters, the value of α is set on the assumption that the wild-type contraction parameter value χ is sufficient to allow full division with the capacity to lose 15% of its value before division behaviour is affected. In Figure 5, the initiation threshold α is set to 20,000. The value of α determines the peak of the threshold curve or the "completion threshold".

4.1 Predicting division behaviour in cells depleted of FtsA or ZipA

Deletion of an anchor protein in CAM-FF alters the values of B, the total number of membrane-binding anchors, P_a, the probability that one FtsZ subunit is adjacent to a binding site and the initiation threshold α. Anchor deletion results in an increase in the initiation threshold value α from the assigned wild-type value since $\alpha \propto 1/P_a$. The underlying reason for this behaviour can be understood from Equation (26). The maximum tension the ring may withstand, $\hat{\tau}$, is proportional to P_a so in the deletion mutant, $\hat{\tau}$ is smaller than in the wild-type for a given population of membrane-bound FtsZ. It is therefore less likely that the condition for contraction is met *i.e.* that $\hat{\tau} > \tau_Z$ for lower values of P_a, see Equation (27), and the threshold α is correspondingly increased, see Equation (29).

If FtsA is depleted, as shown in Figure 6C ($B = 450$, $P_a = 0.029$), we expect the initiation threshold to increase to $\alpha = 29,665$ and outcome (ii) is predicted: division is initiated but stalls prior to completion. The predicted average membrane-bound FtsZ polymer length remains at 14 subunits but the percentage incorporation falls to 21%. Experimental data for a mutant with FtsA depleted shows that the Z-ring is still formed, indentations are observed above the Z-ring but division is prevented,[44] in accord with the model prediction that division is initiated but later arrested.

The loss of ZipA changes the parameters to $B = 222$, $P_a = 0.014$, and the effect is shown in Figure 6D. The initiation threshold increases to $\alpha = 61,429$ and the equilibrium value of the contraction parameter falls below the initiation threshold. Outcome (iii) is therefore predicted: division is not initiated. The average membrane-bound FtsZ polymer length is increased slightly to 15 subunits and the percentage incorporation is less than half that of the wild-type at 12%. Following induced ZipA depletion in *E. coli*, cells are no longer able to divide and appear completely smooth.[44] The model thus explains the outcome of ZipA deletion.

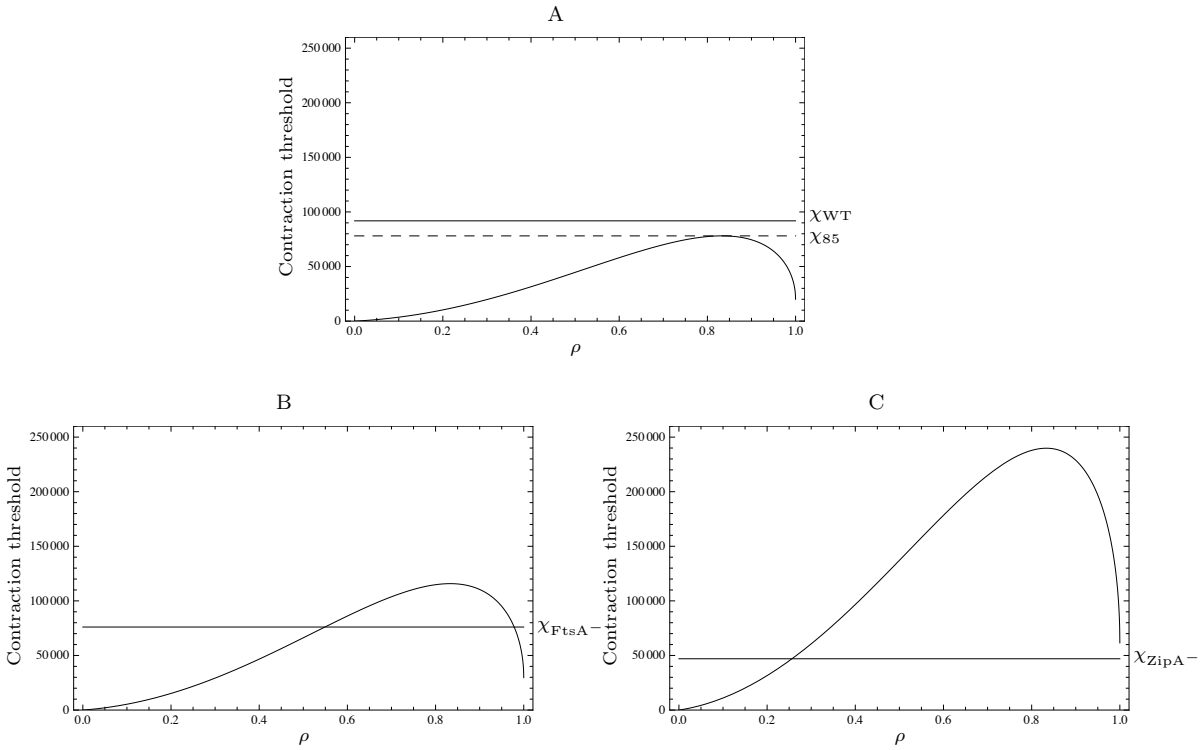

Fig. 6 The effect of anchor deletion. (A) The wild-type value of the contraction parameter χ_{WT} is shown for $B = 672$, $\mathrm{P}_a = 0.043$. χ_{85} indicates the 15% tolerance threshold used to set $\alpha = 20,000$. (B) For the deletion of FtsA ($B = 450$, $\mathrm{P}_a = 0.029$, $\alpha = 29,655$), division is initiated but stalls prior to completion. (C) For the deletion of ZipA ($B = 222$, $\mathrm{P}_a = 0.014$, $\alpha = 61,429$), division is not initiated. All other parameters as shown in Table 1.

5 Analysis of model assumptions

5.1 Membrane-binding

Although the model accurately predicted the ability of the cell to divide in the absence of either one of the anchor proteins, more subtle features may become apparent if we acknowledge that the interaction of FtsZ with each protein is likely to differ, including the value of the dissociation constant κ, the force of the interaction F, and the strength of the interaction of the anchor protein with the cell membrane. It was assumed in the calculation of the maximum tension sustainable by the Z-ring that the weak point is the interaction of FtsZ with the anchor protein. While this seems plausible for the transmembrane protein ZipA,[44] whether this is the case for FtsA is less clear since FtsA is a peripheral membrane protein.[29] An additional anchoring role may be provided by the FtsEX complex.[37] Here, the weak point may be the interaction between FtsE and FtsX. The fact that the model predicts the behaviour of depletion mutants supports our assumptions.

5.2 Polymerisation and dissociation rates

We (and Surovtsev *et al.*[14]) assumed (i) the rate of polymerisation of GDP-bound FtsZ is zero, and (ii) the GTP hydrolysis event results in the dissociation of an FtsZ subunit, thus breaking two FtsZ-FtsZ interfaces. In reality, there may be some level of polymerisation of GDP-bound FtsZ and the hydrolysis event may disrupt only the FtsZ-FtsZ interface containing the bound nucleotide resulting in the dissociation of the parent polymer into two shorter polymers, without the loss of the GDP-bound subunit. While Surovtsev *et al.*[14] assumed that the dissociation of the GDP-bound subunit is instantaneous (thus all subunits in FtsZ polymers were assumed to be GTP-bound), we introduced the rate constant of FtsZ dissociation (following GTP hydrolysis) in accordance with the GTP turnover measured by Romberg and Mitchison[25]. Although technically within CAM-FF all FtsZ subunits within polymers are GTP-bound, apparently in contrast to the report that *in vitro* approximately 20% of the subunits in FtsZ polymers are GDP-bound, the reduced rate constant accounts for the time spent in the GDP-bound state following GTP hydrolysis.

We also assumed that the rate of GTP hydroly-

sis/dissociation is equal for soluble and membrane-bound FtsZ and that the rate of nucleotide exchange for FtsZ subunits within polymers is zero. According to structural studies by Oliva *et al.*[45], and molecular modelling by Mingorance *et al.*[46], the active site is non-occluded leaving the nucleotide free to exchange with the cytosol from within FtsZ polymers. However, Chen and Erickson[47] found no evidence of nucleotide exchange within FtsZ polymers and Huecas *et al.*[48] reported that while exchange can occur, disassembly occurs first. Therefore our assumption is in accord with the latest experimental evidence. We do not explicitly include the role of the putative bundling and stabilising (reduced GTPase activity) proteins that also localise to the Z-ring such as the ZapA orthologue YgfE in *E. coli*.[49,50] Since at this point in time, experimental data to refine the model are not available. Thus we are implicitly assuming that they are behaving as required.

5.3 Regulation of FtsZ localisation

In CAM-FF, we assumed that FtsZ interacts with anchor proteins within the midcell region only, even though the midcell membrane contains only 30% of the total cell complement of anchors. *In vivo*, this apparently unrealistic assumption is made valid by additional systems that operate to regulate the localisation of Z-rings allowing formation at the midcell only.[6]

5.4 Changes in fibre geometry as contraction proceeds

In CAM-FF, we assume that the contraction parameter value χ remains constant throughout the division process. This is unlikely to be true for the later stages of cell division since as the radius decreases, the values of V_{mid} and V_{bnd} also change. The properties of the membrane-bound FtsZ population, including the components of the contraction parameter: the average membrane-bound polymer length and the number of membrane-bound polymers, may also vary. However, it is anticipated that the assumption of constant χ is reasonable for the initial stages of division which actually determines the prediction of division outcome since the peak of the threshold curve *i.e.* the "completion threshold" is early in the division process at $\rho = 0.833$, independent of the value of α.

Finally, a single diffusion constant for all lengths of FtsZ polymer was used. Extension of the current approximation of diffusion to a spatially continuous model may remove the artefact of the rapid assembly time observed compared to that measured *in vivo*. Our model predicts that the assembly of the Z-ring is complete within 5 sec, as does the Surovtsev model.[14] However, the assembly time measured in *E. coli in vivo* is 1 min.[51,52]

5.5 Dynamics of contraction

Whenever the maximal Z-ring tension that can physically be sustained by the population of FtsZ polymers assembled is less than that required to maintain a given radius, the Z-ring radius is expected to expand under the force of the cell surface tension. Conversely, whenever the maximum tension sustainable in the Z-ring exceeds the tension required to maintain a given Z-ring radius, we assume that cell constriction proceeds. The relationship between the rate of change of the Z-ring radius and the difference in the maximal tension and the required tension was assumed to be linear, as shown in Figure 7A. Depending on the molecular mechanism, it is conceivable that the true form of the relationship is non-linear, *e.g.* proportional to $(\tau_Z - \hat{\tau})^3$ as in Figure 7B, or a higher-order power. For the current analysis, the prediction of division outcome is based on the sign of $(\tau_Z - \hat{\tau})$. Therefore, this assumption only concerns the the rate of change of the radius.

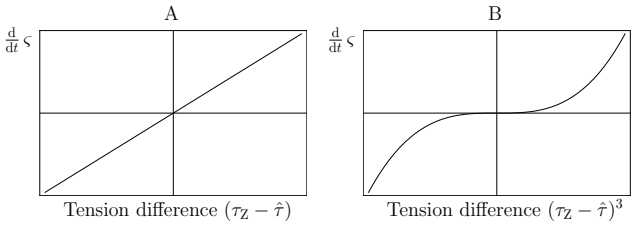

Fig. 7 Relationship between the rate of change of the Z-ring radius ς and the difference in calculated tensions. (A) In the presented model the relationship is assumed to be linear $\frac{d}{dt}\varsigma = \vartheta_0(\tau_Z - \hat{\tau})$. (B) The true form may be a higher order power *e.g.* $\frac{d}{dt}\varsigma = \vartheta_0(\tau_Z - \hat{\tau})^3$.

6 Discussion and conclusions

The model presented here integrates the observed assembly behaviour of FtsZ *in vitro* with the hypothesis that the Z-ring is a molecular assembly of short open polymers that bind to the membrane *via* linking proteins, rather than extremely long cyclic polymers, assumed in earlier work of Surovtsev *et al.*[14]. The division of the cell into distinct compartments and the introduction of diffusion of FtsZ between the cell caps and the midcell region, along with explicitly modelling the attachment of FtsZ polymers to membrane anchors, have been shown to be sufficient to prevent the truncation artefact that arises in the Surovtsev model. The model was further extended by representing the forces of adherence of FtsZ polymers to the cell membrane and their additional role in the generation and support of tension during contraction of the midcell region. This analysis linked the chemical population dynamics of membrane-bound FtsZ polymers to the force of contraction

via the definition of the contraction parameter χ, a useful parameter in the prediction of the ability of cells to initiate and complete cell division.

We used CAM-FF to analyse the effect of reducing the concentrations of membrane-anchoring proteins to understand how their absence inhibits cell division by reducing the number of FtsZ polymers and the percentage of FtsZ molecules in the cell that bind to the membrane. Cell division is still initiated if the less concentrated anchor FtsA is depleted but division stalls before completion. The cells show no sign of even initiating cell division if the more prevalent anchor ZipA is removed. Thus we effectively model whether division occurs or not. More work is required to to accurately model the timescale of cell division. In particular a more complicated analysis of diffusion is required, though currently the experimental parameters are not available.

Our model is silent on the molecular mechanism of Z-ring contraction except to consider the force required for it. At the molecular level, we implied this constriction as being driven by thermodynamic fluctuations. Biochemically analogous processes, such as the contraction of mammalian skeletal muscle, have previously been modelled by a Brownian ratchet mechanism whereby the movement of a motor protein along the actin fibre due to thermal fluctuation becomes unidirectional when coupled to a non-equilibrium chemical reaction.[53] For the contraction of skeletal muscle, the directionality arises from the conformational changes of the motor protein due to its nucleotide-binding state, where the chemical hydrolysis of the nucleotide is far from equilibrium.[54] While no equivalent motor protein has hitherto been identified in prokaryotes, the existence of an as yet undiscovered motor protein is neither proposed nor repudiated in the assumption of a relationship between the difference in calculated tensions and the rate of change of the Z-ring radius. In the absence of a motor protein, as in the presented model, the contraction mechanism is nonetheless coupled to a non-equilibrium process by the continual binding and release of FtsZ polymers, dependent on the rate of GTP-hydrolysis. It seems *prima facie* plausible that the release and rebinding of FtsZ polymers could create a ratchet mechanism whereby local fluctuations become locked in place by the adjacent binding of further FtsZ polymers.

The presence of multiple membrane anchors may provide a ratchet-type mechanism whereby *e.g.* ZipA, and potentially the FtsEX complex, are tightly anchored within the membrane but FtsA is more weakly bound and so may be released and rebound during thermal fluctuations, either from the FtsZ or from the cell membrane. Interestingly, FtsA is an ATPase[55] suggesting a possible means of chemical coupling to drive unidirectional contraction. The state of the bound nucleotide may affect the interaction of FtsA with FtsZ or the cell membrane or both. In our model, we coupled the thermal fluctuations of the Z-ring radius to the non-equilibrium hydrolysis of GTP by FtsZ *via* the rate constant ϑ_0, Equation (28).

An additional role of the Z-ring that is not included in this work is the recruitment of peptidoglycan remodelling enzymes on the outside of the inner cell membrane.[6] As the Z-ring contracts, the peptidoglycan remodelling process potentially creates a physical barrier to any subsequent re-expansion of the Z-ring. This barrier formation process would be a positive feedback loop contributing to unidirectional contraction by consolidating the progress made thus far. The mechanics of the bacterial cell wall during division have been modelled by Lan *et al.*[20] in a complementary study. We assume that the contraction parameter is constant at the initial stages of division which is satisfactory for the prediction of incomplete cell division but to be fully confident of the prediction of division, the cell wall must also be considered.

We have established a framework for the further investigation of the effect of modifications to the biochemical properties of FtsZ and its membrane binding on the initiation and completion of cell division. Application of such a framework will not only improve our understanding of the biological process itself, but may also be applied to the optimisation of antibiotic drug design. Potential drug interactions may be tested for efficacy *in silico* by identification of their effect on key processes of the system. This model may also now be applied to a global model of cell division as proposed by Surovtsev *et al.*[19].

A ODEs as defined by Surovtsev *et al.*[14]

The change in concentrations of FtsZ molecules over time was given by Surovtsev *et al.*[14] in terms of the following rate equations:

$$\frac{\mathrm{d}}{\mathrm{d}t}Z_\mathrm{D} = -R_\mathrm{ex1} + R_\mathrm{ex2} + R^2_\mathrm{hyd} + R^2_\mathrm{hyd\_cyc} + \xi\sum_{j=3}^{i_\mathrm{max}}\left(R^j_\mathrm{hyd} + R^j_\mathrm{hyd\_cyc}\right), \tag{A.1}$$

$$\frac{\mathrm{d}}{\mathrm{d}t}Z_\mathrm{T} = R_\mathrm{ex1} - R_\mathrm{ex2} - 2R_\mathrm{dim1} + 2R_\mathrm{dim2} - R^2_\mathrm{el1} + \xi R^2_\mathrm{el2} - \xi\sum_{j=3}^{i_\mathrm{max}-1}\left(R^j_\mathrm{el1} - R^j_\mathrm{el2}\right) + R^2_\mathrm{hyd} + \xi R^3_\mathrm{hyd} + \xi\sum_{j=4}^{i_\mathrm{max}}\frac{2}{j-1}R^j_\mathrm{hyd} + R^2_\mathrm{hyd\_cyc}, \tag{A.2}$$

$$\frac{\mathrm{d}}{\mathrm{d}t}Z_2 = R_\mathrm{dim1} - R_\mathrm{dim2} - R^2_\mathrm{el1} + \xi R^2_\mathrm{el2} - R^2_\mathrm{an2} - R^2_\mathrm{cyc1} + R^2_\mathrm{cyc2} - R^2_\mathrm{hyd} + \frac{1}{2}\xi R^3_\mathrm{hyd} + \xi\sum_{j=4}^{i_\mathrm{max}}\frac{2}{j-1}R^j_\mathrm{hyd} + \xi R^3_\mathrm{hyd\_cyc}, \tag{A.3}$$

$$\frac{\mathrm{d}}{\mathrm{d}t}Z_3 = \frac{1}{\xi}R^2_{\mathrm{el1}} - R^2_{\mathrm{el2}} - R^3_{\mathrm{el1}} + R^3_{\mathrm{el2}} - R^3_{\mathrm{an2}} - R^3_{\mathrm{cyc1}} + R^3_{\mathrm{cyc2}} - R^3_{\mathrm{hyd}} + \frac{1}{3}R^4_{\mathrm{hyd}} + \sum_{j=5}^{i_{\max}} \frac{2}{j-1}R^j_{\mathrm{hyd}} + R^4_{\mathrm{hyd\_cyc}} \,, \quad \text{(A.4)}$$

$$\frac{\mathrm{d}}{\mathrm{d}t}Z_i = R^{i-1}_{\mathrm{el1}} - R^{i-1}_{\mathrm{el2}} - R^i_{\mathrm{el1}} + R^i_{\mathrm{el2}} + R^i_{\mathrm{an1}} - R^i_{\mathrm{an2}} - R^i_{\mathrm{cyc1}} + R^i_{\mathrm{cyc2}} - R^i_{\mathrm{hyd}} + \frac{1}{i}R^{i+1}_{\mathrm{hyd}} + \sum_{j=i+2}^{i_{\max}} \frac{2}{j-1}R^j_{\mathrm{hyd}} + R^{i+1}_{\mathrm{hyd\_cyc}} \,, \qquad i = 4 \ldots i = i_{\max} - 2 \,, \quad \text{(A.5)}$$

$$\frac{\mathrm{d}}{\mathrm{d}t}Z_{i_{\max}-1} = R^{i_{\max}-2}_{\mathrm{el1}} - R^{i_{\max}-2}_{\mathrm{el2}} - R^{i_{\max}-1}_{\mathrm{el1}} + R^{i_{\max}-1}_{\mathrm{el2}} + R^{i_{\max}-1}_{\mathrm{an1}} - R^{i_{\max}-1}_{\mathrm{cyc1}} + R^{i_{\max}-1}_{\mathrm{cyc2}} - R^{i_{\max}-1}_{\mathrm{hyd}} + \frac{1}{i_{\max}-1}R^{i_{\max}}_{\mathrm{hyd}} + R^{i_{\max}}_{\mathrm{hyd\_cyc}} \,, \quad \text{(A.6)}$$

$$\frac{\mathrm{d}}{\mathrm{d}t}Z_{i_{\max}} = R^{i_{\max}-1}_{\mathrm{el1}} - R^{i_{\max}-1}_{\mathrm{el2}} + R^{i_{\max}}_{\mathrm{an1}} - R^{i_{\max}}_{\mathrm{cyc1}} + R^{i_{\max}}_{\mathrm{cyc2}} - R^{i_{\max}}_{\mathrm{hyd}} \quad \text{(A.7)}$$

and

$$\frac{\mathrm{d}}{\mathrm{d}t}Z^{\mathrm{cyc}}_i = R^i_{\mathrm{cyc1}} - R^i_{\mathrm{cyc2}} - R^i_{\mathrm{hyd\_cyc1}} \,. \quad \text{(A.8)}$$

ξ is the ratio of the midcell volume to the cytosol volume.

To allow polymers to form closed rings, the forward and reverse cyclisation rates are given by

$$R^i_{\mathrm{cyc1}} = k_{\mathrm{cyc1}}(i)\,Z_i \,,\; R^i_{\mathrm{cyc2}} = k_{\mathrm{cyc2}}\,Z^{\mathrm{cyc}}_i \,, \quad \text{(A.9)}$$

where the forward rate constant is dependent on the polymer length i and is given by

$$k_{\mathrm{cyc1}}(i) = k_{\mathrm{cyc1}}\,e^{-(i-i_0)^2/\sigma^2} \,, \quad \text{(A.10)}$$

where i_0 is the length at which the cyclisation rate is optimal and σ is the width of the distribution of rates. The rate of GTP hydrolysis for cyclic polymers is given by

$$R^i_{\mathrm{hyd\_cyc}} = i\,k_{\mathrm{hyd}}\,Z^{\mathrm{cyc}}_i \,, \quad \text{(A.11)}$$

where cyclic polymers of length i have i GTPase active sites.

B ODEs of the present model

The change in concentration of FtsZ molecules within the cell caps over time is given by

$$\frac{\mathrm{d}}{\mathrm{d}t}Z^{\mathrm{cc}}_{\mathrm{D}} = -R_{\mathrm{ex1}} + R_{\mathrm{ex2}} + \sum_{j=2}^{i_{\max}} R^j_{\mathrm{dis}} + R^{\mathrm{D}}_{\mathrm{mc}} \,, \quad \text{(B.1)}$$

$$\frac{\mathrm{d}}{\mathrm{d}t}Z^{\mathrm{cc}}_{\mathrm{T}} = R_{\mathrm{ex1}} - R_{\mathrm{ex2}} - 2R_{\mathrm{dim1}} + 2R_{\mathrm{dim2}} - \sum_{j=2}^{i_{\max-1}} (R^j_{\mathrm{el1}} - R^j_{\mathrm{el2}}) + R^2_{\mathrm{dis}} + \sum_{j=3}^{i_{\max}} \frac{2}{j-1}R^j_{\mathrm{dis}} + R^{\mathrm{T}}_{\mathrm{mc}} \,, \quad \text{(B.2)}$$

$$\frac{\mathrm{d}}{\mathrm{d}t}Z^{\mathrm{cc}}_2 = R_{\mathrm{dim1}} - R_{\mathrm{dim2}} - R^2_{\mathrm{el1}} + R^2_{\mathrm{el2}} - R^2_{\mathrm{an2}} - R^2_{\mathrm{dis}} + \frac{1}{2}R^3_{\mathrm{dis}} + \sum_{j=4}^{i_{\max}} \frac{2}{j-1}R^j_{\mathrm{dis}} + R^2_{\mathrm{mc}} \,, \quad \text{(B.3)}$$

$$\frac{\mathrm{d}}{\mathrm{d}t}Z^{\mathrm{cc}}_i = R^{i-1}_{\mathrm{el1}} - R^{i-1}_{\mathrm{el2}} - R^i_{\mathrm{el1}} + R^i_{\mathrm{el2}} + R^i_{\mathrm{an1}} - R^i_{\mathrm{an2}} - R^i_{\mathrm{dis}} + \frac{1}{i}R^{i+1}_{\mathrm{dis}} + \sum_{j=i+2}^{i_{\max}} \frac{2}{j-1}R^j_{\mathrm{dis}} + R^i_{\mathrm{mc}} \,, \qquad i = 3 \ldots i = i_{\max} - 2 \,, \quad \text{(B.4)}$$

$$\frac{\mathrm{d}}{\mathrm{d}t}Z^{\mathrm{cc}}_{i_{\max}-1} = R^{i_{\max}-2}_{\mathrm{el1}} - R^{i_{\max}-2}_{\mathrm{el2}} - R^{i_{\max}-1}_{\mathrm{el1}} + R^{i_{\max}-1}_{\mathrm{el2}} + R^{i_{\max}-1}_{\mathrm{an1}} - R^{i_{\max}-1}_{\mathrm{dis}} + \frac{1}{i_{\max}-1}R^{i_{\max}}_{\mathrm{dis}} + R^{i_{\max}-1}_{\mathrm{mc}} \quad \text{(B.5)}$$

and

$$\frac{\mathrm{d}}{\mathrm{d}t}Z^{\mathrm{cc}}_{i_{\max}} = R^{i_{\max}-1}_{\mathrm{el1}} - R^{i_{\max}-1}_{\mathrm{el2}} + R^{i_{\max}}_{\mathrm{an1}} - R^{i_{\max}}_{\mathrm{dis}} + R^{i_{\max}}_{\mathrm{mc}} \,. \quad \text{(B.6)}$$

For the midcell compartment the change in concentration of FtsZ molecules over time is given by

$$\frac{\mathrm{d}}{\mathrm{d}t}Z^{\mathrm{mid}}_{\mathrm{D}} = -R_{\mathrm{ex1}} + R_{\mathrm{ex2}} + \sum_{j=2}^{i_{\max}} R^j_{\mathrm{dis}} + R^{\mathrm{D}}_{\mathrm{cm}} - R^{\mathrm{D}}_{\mathrm{bind1}} + \frac{V_{\mathrm{bnd}}}{V_{\mathrm{mid}}}R^{\mathrm{D}}_{\mathrm{bind2}} + \frac{V_{\mathrm{bnd}}}{V_{\mathrm{mid}}}\sum_{j=2}^{i_{\max}} \mathrm{P}_1(\text{no sites} \mid i' = j)R^j_{\mathrm{dis\_bnd}} \,, \quad \text{(B.7)}$$

$$\frac{\mathrm{d}}{\mathrm{d}t}Z_{\mathrm{T}}^{\mathrm{mid}} = R_{\mathrm{ex1}} - R_{\mathrm{ex2}} - 2R_{\mathrm{dim1}} + 2R_{\mathrm{dim2}} - \frac{V_{\mathrm{bnd}}}{V_{\mathrm{mid}}}R_{\mathrm{dim1\_bnd}} + \frac{V_{\mathrm{bnd}}}{V_{\mathrm{mid}}}R_{\mathrm{dim2\_bnd}} - \sum_{j=2}^{i_{\mathrm{max}}-1}(R_{\mathrm{el1}}^{j} - R_{\mathrm{el2}}^{j}) - \frac{V_{\mathrm{bnd}}}{V_{\mathrm{mid}}}\sum_{j=2}^{i_{\mathrm{max}}-1}(R_{\mathrm{el1\_bnd}}^{j} - R_{\mathrm{el2\_bnd}}^{j}) + R_{\mathrm{dis}}^{2} + \sum_{j=3}^{i_{\mathrm{max}}}\frac{2}{j-1}R_{\mathrm{dis}}^{j} + R_{\mathrm{cm}}^{\mathrm{T}} - R_{\mathrm{bind1}}^{\mathrm{T}} + \frac{V_{\mathrm{bnd}}}{V_{\mathrm{mid}}}R_{\mathrm{bind2}}^{\mathrm{T}} + \frac{V_{\mathrm{bnd}}}{V_{\mathrm{mid}}}\mathrm{P}_1(\text{no sites} \mid i' = 2)R_{\mathrm{dis\_bnd}}^{2} + \frac{V_{\mathrm{bnd}}}{V_{\mathrm{mid}}}\sum_{j=3}^{i_{\mathrm{max}}}\frac{2}{j-1}\mathrm{P}_1(\text{no sites} \mid i' = j)R_{\mathrm{dis\_bnd}}^{j}\,, \tag{B.8}$$

$$\frac{\mathrm{d}}{\mathrm{d}t}Z_{2}^{\mathrm{mid}} = R_{\mathrm{dim1}} - R_{\mathrm{dim2}} - R_{\mathrm{el1}}^{2} + R_{\mathrm{el2}}^{2} - R_{\mathrm{an2}}^{2} - R_{\mathrm{an2\_mid}}^{2} - R_{\mathrm{dis}}^{2} + \frac{1}{2}R_{\mathrm{dis}}^{3} + \sum_{j=4}^{i_{\mathrm{max}}}\frac{2}{j-1}R_{\mathrm{dis}}^{j} + R_{\mathrm{cm}}^{2} - R_{\mathrm{bind1}}^{2} + \frac{V_{\mathrm{bnd}}}{V_{\mathrm{mid}}}R_{\mathrm{bind2}}^{2} + \frac{1}{2}\cdot\frac{V_{\mathrm{bnd}}}{V_{\mathrm{mid}}}\mathrm{P}_2(\text{no sites} \mid i' = 3)R_{\mathrm{dis\_bnd}}^{3} + \frac{V_{\mathrm{bnd}}}{V_{\mathrm{mid}}}\sum_{j=4}^{i_{\mathrm{max}}}\frac{2}{j-1}\mathrm{P}_2(\text{no sites} \mid i' = j)R_{\mathrm{dis\_bnd}}^{j}\,, \tag{B.9}$$

$$\frac{\mathrm{d}}{\mathrm{d}t}Z_{i}^{\mathrm{mid}} = R_{\mathrm{el1}}^{i-1} - R_{\mathrm{el2}}^{i-1} - R_{\mathrm{el1}}^{i} + R_{\mathrm{el2}}^{i} + R_{\mathrm{an1}}^{i} - R_{\mathrm{an2}}^{i} - R_{\mathrm{an2\_mid}}^{i} - R_{\mathrm{dis}}^{i} + \frac{1}{i}R_{\mathrm{dis}}^{i+1} + \sum_{j=i+2}^{i_{\mathrm{max}}}\frac{2}{j-1}R_{\mathrm{dis}}^{j} + R_{\mathrm{cm}}^{i} - R_{\mathrm{bind1}}^{i} + \frac{V_{\mathrm{bnd}}}{V_{\mathrm{mid}}}R_{\mathrm{bind2}}^{i} + \frac{1}{i}\cdot\frac{V_{\mathrm{bnd}}}{V_{\mathrm{mid}}}\mathrm{P}_i(\text{no sites} \mid i' = i+1)R_{\mathrm{dis\_bnd}}^{i+1} + \frac{V_{\mathrm{bnd}}}{V_{\mathrm{mid}}}\sum_{j=i+2}^{i_{\mathrm{max}}}\frac{2}{j-1}\mathrm{P}_i(\text{no sites} \mid i' = j)R_{\mathrm{dis\_bnd}}^{j}\,, \quad i = 3 \ldots i = i_{\mathrm{max}} - 2\,, \tag{B.10}$$

$$\frac{\mathrm{d}}{\mathrm{d}t}Z_{i_{\mathrm{max}}-1}^{\mathrm{mid}} = R_{\mathrm{el1}}^{i_{\mathrm{max}}-2} - R_{\mathrm{el2}}^{i_{\mathrm{max}}-2} - R_{\mathrm{el1}}^{i_{\mathrm{max}}-1} + R_{\mathrm{el2}}^{i_{\mathrm{max}}-1} + R_{\mathrm{an1}}^{i_{\mathrm{max}}-1} - R_{\mathrm{dis}}^{i_{\mathrm{max}}-1} + \frac{1}{i_{\mathrm{max}}-1}R_{\mathrm{dis}}^{i_{\mathrm{max}}} + R_{\mathrm{cm}}^{i_{\mathrm{max}}-1} - R_{\mathrm{bind1}}^{i_{\mathrm{max}}-1} + \frac{V_{\mathrm{bnd}}}{V_{\mathrm{mid}}}R_{\mathrm{bind2}}^{i_{\mathrm{max}}-1} + \frac{1}{i_{\mathrm{max}}-1}\cdot\frac{V_{\mathrm{bnd}}}{V_{\mathrm{mid}}}\mathrm{P}_{i_{\mathrm{max}}-1}(\text{no sites} \mid i' = i_{\mathrm{max}})R_{\mathrm{dis\_bnd}}^{i_{\mathrm{max}}} \tag{B.11}$$

and

$$\frac{\mathrm{d}}{\mathrm{d}t}Z_{i_{\mathrm{max}}}^{\mathrm{mid}} = R_{\mathrm{el1}}^{i_{\mathrm{max}}-1} - R_{\mathrm{el2}}^{i_{\mathrm{max}}-1} + R_{\mathrm{an1}}^{i_{\mathrm{max}}} - R_{\mathrm{dis}}^{i_{\mathrm{max}}} + R_{\mathrm{mc}}^{i_{\mathrm{max}}} - R_{\mathrm{bind1}}^{i_{\mathrm{max}}} + \frac{V_{\mathrm{bnd}}}{V_{\mathrm{mid}}}R_{\mathrm{bind2}}^{i_{\mathrm{max}}}\,, \tag{B.12}$$

where V_{mid} and V_{bnd} are the volume of the midcell and the midecell membrane compartments, respectively. A volume is used for the midcell membrane compartment rather than a surface area so that the concentrations of membrane-bound molecules are in equivalent dimensions to the cell caps and midcell concentrations, and so the global rate constants may be applied.

For the midcell membrane, the change in concentration of FtsZ molecules over time is given by

$$\frac{\mathrm{d}}{\mathrm{d}t}Z_{\mathrm{D}}^{\mathrm{bnd}} = \frac{V_{\mathrm{mid}}}{V_{\mathrm{bnd}}}R_{\mathrm{bind1}}^{\mathrm{D}} - R_{\mathrm{bind2}}^{\mathrm{D}} - R_{\mathrm{ex1}} + R_{\mathrm{ex2}} + \sum_{j=2}^{i_{\mathrm{max}}}(1 - \mathrm{P}_1(\text{no sites} \mid i' = j))R_{\mathrm{dis\_bnd}}^{j}\,, \tag{B.13}$$

$$\frac{\mathrm{d}}{\mathrm{d}t}Z_{\mathrm{T}}^{\mathrm{bnd}} = \frac{V_{\mathrm{mid}}}{V_{\mathrm{bnd}}}R_{\mathrm{bind1}}^{\mathrm{T}} - R_{\mathrm{bind2}}^{\mathrm{T}} + R_{\mathrm{ex1}} - R_{\mathrm{ex2}} - R_{\mathrm{dim1\_bnd}} + R_{\mathrm{dim2\_bnd}} + (1 - \mathrm{P}_1(\text{no sites} \mid i' = 2))R_{\mathrm{dis\_bnd}}^{2} + \sum_{j=3}^{i_{\mathrm{max}}}\frac{2}{j-1}(1 - \mathrm{P}_1(\text{no sites} \mid i' = j))R_{\mathrm{dis\_bnd}}^{j}\,, \tag{B.14}$$

$$\frac{\mathrm{d}}{\mathrm{d}t}Z_{2}^{\mathrm{bnd}} = \frac{V_{\mathrm{mid}}}{V_{\mathrm{bnd}}}R_{\mathrm{bind1}}^{2} - R_{\mathrm{bind2}}^{2} + R_{\mathrm{dim1\_bnd}} - R_{\mathrm{dim2\_bnd}} - R_{\mathrm{el1\_bnd}}^{2} + R_{\mathrm{el2\_bnd}}^{2} - R_{\mathrm{an2\_bnd}}^{2} - R_{\mathrm{dis\_bnd}}^{2} + \frac{1}{2}\cdot(1 - \mathrm{P}_2(\text{no sites} \mid i' = 3))R_{\mathrm{dis\_bnd}}^{3} + \sum_{j=4}^{i_{\mathrm{max}}}\frac{2}{j-1}(1 - \mathrm{P}_i(\text{no sites} \mid i' = j))R_{\mathrm{dis\_bnd}}^{j}\,, \tag{B.15}$$

$$\frac{\mathrm{d}}{\mathrm{d}t}Z_{\mathrm{i}}^{\mathrm{bnd}} = \frac{V_{\mathrm{mid}}}{V_{\mathrm{bnd}}}R_{\mathrm{bind1}}^{i} - R_{\mathrm{bind2}}^{i} + R_{\mathrm{el1\_bnd}}^{i-1} - R_{\mathrm{el2\_bnd}}^{i-1} - R_{\mathrm{el1\_bnd}}^{i} + R_{\mathrm{el2\_bnd}}^{i} + R_{\mathrm{an1\_bnd}}^{i} - R_{\mathrm{an2\_bnd}}^{i} - R_{\mathrm{dis\_bnd}}^{i} + \frac{1}{i}.(1-\mathrm{P}_i(\text{no sites} \mid i'=i+1))R_{\mathrm{dis\_bnd}}^{i+1} + \sum_{j=i+2}^{i_{\max}} \frac{2}{j-1}(1-\mathrm{P}_i(\text{no sites} \mid i'=j))R_{\mathrm{dis\_bnd}}^{j}\,, \quad i=3\ldots i=i_{\max}-2\,, \tag{B.16}$$

$$\frac{\mathrm{d}}{\mathrm{d}t}Z_{i_{\max}-1}^{\mathrm{bnd}} = \frac{V_{\mathrm{mid}}}{V_{\mathrm{bnd}}}R_{\mathrm{bind1}}^{i_{\max}-1} - R_{\mathrm{bind2}}^{i_{\max}-1} + R_{\mathrm{el1\_bnd}}^{i_{\max}-2} - R_{\mathrm{el2\_bnd}}^{i_{\max}-2} - R_{\mathrm{el1\_bnd}}^{i_{\max}-1} + R_{\mathrm{el2\_bnd}}^{i_{\max}-1} + R_{\mathrm{an1\_bnd}}^{i_{\max}-1} - R_{\mathrm{dis\_bnd}}^{i_{\max}-1} + \frac{1}{i_{\max}-1}.(1-\mathrm{P}_{i_{\max}-1}(\text{no sites} \mid i'=i_{\max}))R_{\mathrm{dis\_bnd}}^{i_{\max}} \tag{B.17}$$

and

$$\frac{\mathrm{d}}{\mathrm{d}t}Z_{i_{\max}}^{\mathrm{bnd}} = \frac{V_{\mathrm{mid}}}{V_{\mathrm{bnd}}}R_{\mathrm{bind1}}^{i_{\max}} - R_{\mathrm{bind2}}^{i_{\max}} + R_{\mathrm{el1\_bnd}}^{i_{\max}-1} - R_{\mathrm{el2\_bnd}}^{i_{\max}-1} + R_{\mathrm{an1\_bnd}}^{i_{\max}} - R_{\mathrm{dis\_bnd}}^{i_{\max}}\,. \tag{B.18}$$

The average polymer length $\bar{i}$, the total number of FtsZ polymers N_{Z}, and the total FtsZ concentration Z_{tot} are tracked over time for each compartment given by

$$\bar{i} = \sum_{i=1}^{i_{max}} i Z_i \Bigg/ \sum_{i=1}^{i_{max}} Z_i\,, \tag{B.19}$$

$$N_{\mathrm{Z}} = V_{\mathrm{bnd}}\frac{N_{\mathrm{A}}}{10^{21}}\sum_{i=1}^{i_{max}} Z_i \tag{B.20}$$

and

$$Z_{\mathrm{tot}} = \sum_{i=1}^{i_{max}} i Z_i\,, \tag{B.21}$$

respectively, where Z_1 includes both GDP- and GTP-bound monomers and N_{A} is Avogadro's number.

C Attachment to multiple binding sites

The attachment of an FtsZ polymer to multiple binding sites has been modelled as a Markov chain with state variables x_1 to x_j, where j is the maximum number of binding sites available to the chain. This is illustrated in Figure C 1.

A transition event up the chain is given by the rate of attachment per binding site and the number of free binding sites remaining. Conversely, a transition event down the chain is given by the rate of release per binding site and the number of

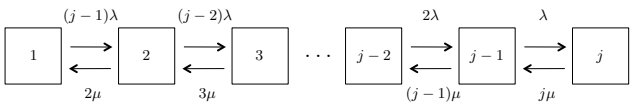

Fig. C 1 Binding to multiple sites. As multiple binding sites are available to a single polymer chain, binding is modelled as a Markov chain where j is the maximum number of binding sites available. λ is the rate of association of FtsZ and a binding site and μ is the rate of dissociation.

sites currently occupied. At equilibrium, the rates of the forward and reverse transition events for x_{j-1} and x_j are equal,

$$j\,\mu\,x_j = \lambda\,x_{j-1}\,. \tag{C.1}$$

For the subsequent pair in the chain, x_{j-2} and x_{j-1},

$$(j-1)\,\mu\,x_{j-1} + \lambda\,x_{j-1} = 2\lambda\,x_{j-2} + j\,\mu\,x_j\,. \tag{C.2}$$

As $j\,\mu\,x_j$ and $\lambda\,x_{j-1}$ are equal then

$$(j-1)\,\mu\,x_{j-1} = 2\lambda\,x_{j-2}\,, \tag{C.3}$$

and

$$x_{j-2} = \frac{(j-1)}{2}\,\kappa x_{j-1}\,, \tag{C.4}$$

where $\kappa = \mu/\lambda$. Continuing in this way for the pair x_{j-3} and x_{j-2} gives

$$x_{j-3} = \frac{(j-2)}{3}\,\kappa x_{j-2}\,, \tag{C.5}$$

and for any subsequent pair this can be generalised to

$$x_{j-\ell} = \frac{(j-\ell+1)}{\ell}\,\kappa x_{j-\ell+1}\,, \tag{C.6}$$

where expression is in terms of the previous term in the sequence. To derive $x_{j-\ell}$ in terms of x_j and κ, each term from $\ell = 1$ is considered. As $x_{j-1} = j\,\kappa x_j$, then substituting into (C.4) for x_{j-2} gives

$$x_{j-2} = j\,\frac{(j-1)}{2}\,\kappa^2 x_j\,. \tag{C.7}$$

Continuing for x_{j-3} gives

$$x_{j-3} = j\,\frac{(j-1)}{2}.\frac{(j-2)}{3}\,\kappa^3 x_j\,, \tag{C.8}$$

so this can be generalised to give $x_{j-\ell}$ in terms of x_j,

$$x_{j-\ell} = \binom{j}{\ell}\,\kappa^{\ell} x_j\,. \tag{C.9}$$

Of interest to the dissociation rate is the fraction of polymers in the singly-bound state. Therefore, this fraction is given by x_1/x_{T} where x_1 can be given by substituting $j-\ell = 1$,

$$x_1 = \binom{j}{j-1}\,\kappa^{j-1} x_j\,, \tag{C.10}$$

which simplifies to

$$x_1 = j\,\kappa^{j-1}\,x_j\,. \tag{C.11}$$

If x_T is the sum of all values of $x_{j-\ell}$ for $\ell = 0$ to $\ell = j-1$ then

$$x_\mathrm{T} = \left[\sum_{\ell=0}^{j-1}\binom{j}{\ell}\,\kappa^{\ell}\right] x_j\,. \tag{C.12}$$

By the binomial theorem, this is equal to

$$((1+\kappa)^j - \kappa^j)\,x_j\,. \tag{C.13}$$

Therefore, taking the value of x_1 from Equation (C.11), as a fraction of x_T given in Equation (C.13), the fraction of polymers expected to be bound by a single binding site when j binding sites are available is given by

$$f_1^j = \frac{j\,\kappa^{j-1}\,x_j}{((1+\kappa)^j - \kappa^j)\,x_j}\,, \tag{C.14}$$

which cancels and rearranges to give

$$f_1^j = \frac{j}{\kappa(1+\frac{1}{\kappa})^j - \kappa}\,, \tag{C.15}$$

as given in Equation (14) of §2.2.2.

D Forces acting on the Z-ring

The contraction process draws the cell membrane inwards, against the outward force from the cell surface tension. The aim of this model is to define the tension of the Z-ring during contraction and the maximum tension the Z-ring can withstand at a given ring radius. Figure D1 shows the components of the cell surface tension τ_0 as the ring constricts. The Z-ring is modelled as a cylinder with length ω and initial radius r. During contraction, the radius of the cylinder decreases where ς is defined as the Z-ring radius at time t of contraction, and ρ is the dimensionless ratio of the contraction radius to the initial radius, $\rho = \varsigma/r$. As can be seen in Figure D1, this ratio is equal to $\sin\beta$. As the ring contracts, the angle β decreases from $\pi/2$ to 0.

The angle β also corresponds to the angle of the tangent to the indented cell surface, with respect to the vertical. This tangent is the resultant of the cell surface tension. Since the pinching tension τ_p balances the vertical component of the surface tension τ_0 at equilibrium, the pinching tension is given by $\tau_0\cos\beta$. To define τ_p in terms of the Z-ring radius, since $\sin\beta = \rho$, the pinching tension is also given by

$$\tau_\mathrm{p} = \tau_0\sqrt{1-\rho^2}\,. \tag{D.1}$$

Since the surface tension acts on both the right and left sides of the cell indentation, the total pinching tension is equal to $2\tau_\mathrm{p}$.

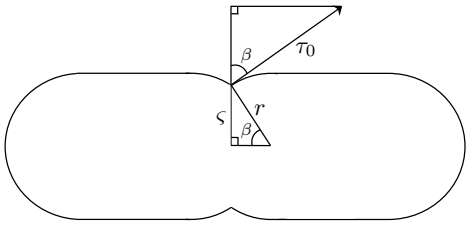

Fig. D 1 Membrane indentation on Z-ring contraction. Z-ring contraction pulls the membrane inwards against the outward force from the cell surface tension τ_0. ς is the radius of the Z-ring at time t of contraction and r is the radius of the Z-ring prior to contraction.

This acts around the circumference of the Z-ring so the pinching force generated is $4\pi\varsigma\,\tau_\mathrm{p}$. This force results in an additional internal pressure over the Z-ring surface area given by

$$\mathrm{P_p} = \frac{4\pi\varsigma\,\tau_\mathrm{p}}{2\pi\varsigma\,\omega}\,, \tag{D.2}$$

which simplifies to

$$\mathrm{P_p} = 2\frac{\tau_p}{\omega}\,. \tag{D.3}$$

To determine the Z-ring tension during contraction τ', the forces acting on either side of a vertical slice through the ring are considered, as shown in Figure D2. The magnitude of the force due to ring tension is given by this tension acting over the length of the two edges created by the slice. At equilibrium, this is balanced by the force of the internal pressure over the cross-sectional area. Therefore

$$2\omega\tau' = 2\varsigma\,\omega\mathrm{P_p}\,, \tag{D.4}$$

and substituting for $\mathrm{P_p}$ given in Equation (D.3) and expressing in terms of the dimensionless ratio ρ,

$$\tau' = \frac{2r}{\omega}\rho\,\tau_\mathrm{p}\,. \tag{D.5}$$

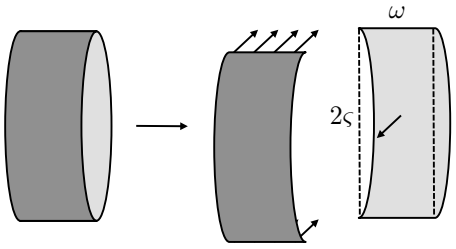

Fig. D 2 Forces acting on the Z-ring. For the slice through the Z-ring, at equilibrium the horizontal force due to the ring tension is balanced by the internal pressure acting over the cross-sectional area of the slice.

If the total Z-ring tension is given by the original cell surface tension plus the additional contraction tension τ' then

$$\tau_{\mathrm{Z}} = \tau_0 \left(1 + \frac{2r}{\omega}\rho\sqrt{1-\rho^2}\right) . \tag{D.6}$$

This is the first key property of the contraction model, the total tension of the Z-ring in terms of the cell surface tension and the radius of the Z-ring during contraction, as given in Equation (25) of §2.2.5.

The second key property is the maximum tension the Z-ring can withstand at a given radius, based on the assembled population of FtsZ polymers. To calculate this tension, a transverse line through the Z-ring is considered. As shown in Figure D3 for polymers bound to the membrane, for a polymer of length l, the probability that the transverse line intersects the polymer is

$$\mathrm{P}(\text{polymer hit} \mid l) = \frac{h}{2\pi\varsigma} , \tag{D.7}$$

where $h = l\sin\varphi$. As angle φ may take any value from 0 to π, the probability that a polymer of length l is intersected by the transverse line is given by

$$\mathrm{P}(\text{polymer hit} \mid l) = \int_0^\pi \frac{l}{2\pi\varsigma}\sin\varphi \,\mathrm{dF}(\varphi) . \tag{D.8}$$

If φ is uniform over $[0\,,\pi]$ then

$$\mathrm{P}(\text{polymer hit} \mid l) = \int_0^\pi \frac{l}{2\pi\varsigma}\sin\varphi \,\frac{1}{\pi}\,\mathrm{d}\varphi , \tag{D.9}$$

which simplifies to

$$\mathrm{P}(\text{polymer hit} \mid l) = \frac{l}{\pi^2\varsigma} , \tag{D.10}$$

since $\int_0^\pi \sin\varphi\,\mathrm{d}\varphi \;= 2$.

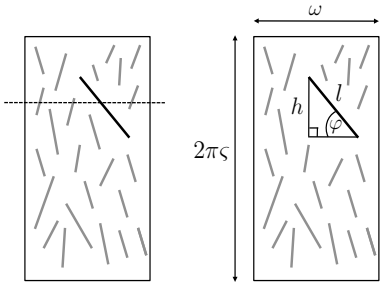

Fig. D 3 FtsZ polymers accumulated at the Z-ring. For a polymer of length l within the Z-ring, the probability that a transverse line intersects is given by $h/2\pi\varsigma$.

To extend this to all polymers, the probability that a polymer molecule is intersected is given by

$$\mathrm{P}(\text{polymer hit}) = \frac{l_0}{\pi^2\varsigma}\sum_{i=1}^{\infty} i\,\mathrm{P}_i, \tag{D.11}$$

where l_0 is the length of one FtsZ subunit, i is the number of subunits in the polymer and P_i is the probability that a polymer has length i subunits. The value of the summation is determined by the population of FtsZ molecules assembled at the Z-ring and bound to the membrane *via* anchors. The probability that a selected polymer has length i subunits is given by the concentration of polymers of length i, divided by the total polymer concentration,

$$\mathrm{P}_i = Z_i \Big/ \sum_{i=1}^{\infty} Z_i . \tag{D.12}$$

Multiplying by the number of subunits, and summing for all values of i gives the average polymer length. Therefore,

$$\sum_{i=1}^{\infty} i\,\mathrm{P}_i = \sum_{i=1}^{\infty} i Z_i \Big/ \sum_{i=1}^{\infty} Z_i = \bar{i} , \tag{D.13}$$

and

$$\mathrm{P}(\text{polymer hit}) = \frac{l_0\,\bar{i}}{\pi^2\varsigma} . \tag{D.14}$$

Since

$$N_{\mathrm{Z}} \triangleq \sum_{i=1}^{\infty} N_i , \tag{D.15}$$

the expectation of the number of polymers intersected by the transverse line is given by

$$\mathbb{E}(\text{number of polymers hit}) = \sum_{i=1}^{\infty} \frac{l_0\,\bar{i}}{\pi^2\varsigma} N_i = \frac{l_0\,\bar{i} N_{\mathrm{Z}}}{\pi^2\varsigma} . \tag{D.16}$$

To calculate the tension through the transverse line, the number of anchors and the maximum force sustainable per anchor is considered. For a polymer intersected by the transverse line, the expectation of the number of anchor sites on one side of the line is given by the number of subunits within the polymer and the probability that a subunit is adjacent to an anchor binding site. Therefore

$$\mathbb{E}(\text{anchors} \mid i) = \frac{1}{2}\,\mathrm{P}_a\, i , \tag{D.17}$$

where the correction factor of

$$\frac{1}{1-(1-\mathrm{P}_a)^i} , \tag{D.18}$$

used previously, has been omitted since this tends to 1 for increasing values of i. The force sustainable, perpendicular to the transverse line is then proportional to the number of anchors and depends on the angle φ so

$$\mathbb{E}(\text{max force} \mid i) \propto \mathbb{E}(\text{anchors} \mid i)\,\frac{1}{\pi}\int_0^\pi \sin\varphi\,\mathrm{d}\varphi . \tag{D.19}$$

Evaluating the integral and substituting for $\mathbb{E}(\text{anchors} \mid i)$ from Equation (D.17) gives

$$\mathbb{E}(\text{max force} \mid i) \propto \frac{\mathrm{P}_a i}{\pi}, \tag{D.20}$$

and for any polymer intersected,

$$\mathbb{E}(\text{max force}) \propto \frac{\mathrm{P}_a \bar{i}}{\pi}. \tag{D.21}$$

This is the expectation of the maximum force sustainable for a single polymer. For the total number of polymers intersected by the transverse line from Equation (D.16), the total maximum force is given by

$$\mathbb{E}(\text{max force of line}) \propto \frac{\mathrm{P}_a \bar{i}}{\pi} \cdot \frac{l_0 \bar{i} N_\mathrm{Z}}{\pi^2 \varsigma} = \frac{\mathrm{P}_a l_0}{\pi^3 r} \cdot \frac{\bar{i}^2 N_\mathrm{Z}}{\rho}. \tag{D.22}$$

The expectation of the maximum tension in the line is then given by the expectation of the maximum force of the line divided by the line length ω,

$$\mathbb{E}(\text{max tension of line}) \propto \frac{\mathrm{P}_a l_0}{\pi^3 \omega r} \cdot \frac{\bar{i}^2 N_\mathrm{Z}}{\rho}. \tag{D.23}$$

On the assumption that the attachment to the anchor is the weak point, the maximum tension $\hat{\tau}$ is given by,

$$\hat{\tau} = F \frac{\mathrm{P}_a l_0}{\omega r} \cdot \frac{\bar{i}^2 N_\mathrm{Z}}{\rho}, \tag{D.24}$$

where F is proportional to the force of the interaction of FtsZ and a single anchor site and accounts for the factor of $1/\pi^3$.

E The present model resolves the truncation artefact of the Surovtsev model[14]

The present model is based on the conceptual division of the cell into three compartments. Surovtsev *et al.* [14] assumed that FtsZ monomers and dimers are dispersed throughout the cell but that polymers of length $i \geq 3$ subunits are located exclusively in the midcell region. However, the two regions were not modelled as separate compartments. Instead, the concentrations of polymers of length $i \geq 3$ were scaled by a factor ξ, the ratio of the midcell volume to the cytosol volume, and reactions proceeded between all the molecules in the system. The Surovtsev ODEs, provided in Appendix A, included terms for nucleotide exchange, dimerisation, elongation, annealing, polymer cyclisation, and GTP hydrolysis reactions, with the factor ξ used to account for any "interfacial" reaction. For example, the increase in the trimer concentration due to dimer elongation was scaled to be 1000 times larger than the corresponding decrease in the dimer concentration.

The scaling factor ξ on the modelled population of FtsZ engenders a truncation artefact: long open polymers accumulate with increasing concentrations towards $i_{\max}$, as shown in Figure E1A. Increasing the value of $i_{\max}$ then shifts the increase in concentration to greater values of i. As a result, the average open polymer length depends on $i_{\max}$. For example, for $i_{\max} = 150$, the average open polymer length is 62 subunits whereas for $i_{\max} = 200$, the average open polymer length is 70 subunits. At such high concentrations of polymers, the value of $i_{\max}$ is not sufficiently high to avoid truncation artefacts, due to their confinement to the midcell region. As can be seen in Figure E1B-D, the artefact is not observed for any of the three compartments in the present model. The average polymer length for the membrane-bound population is considerably lower than in the Surovtsev model[14], at 14 subunits for $i_{\max} = 150$ and if the maximum length is increased to $i_{\max} = 200$, the average membrane-bound polymer length remains at 14 subunits. Thus $i_{\max} = 150$ is sufficiently high to avoid the truncation artefact. Surovtsev *et al.* [14] acknowledge that the value for $i_{\max}$ was fixed at 150 due to limitations of the software used. However, the present model shows that including (i) the diffusion of FtsZ into the midcell region, in a more physically realistic manner, and (ii) an explicit model of FtsZ membrane binding, prevents the truncation artefact and the formation of polymers as long as those in the Surovtsev model[14]. The formation of long polymers was due to the artificial increase in the FtsZ concentration with the confinement to the midcell volume.

References

1 D. Bramhill, *Annual review of cell and developmental biology*, 1997, **13**, 395–424.
2 P. Maupin and T. Pollard, *Journal of ultrastructure and molecular structure research*, 1986, **94**, 92–103.
3 Z. Li, M. Trimble, Y. Brun and G. Jensen, *The EMBO journal*, 2007, **26**, 4694–4708.
4 E. Bi and J. Lutkenhaus, *Nature*, 1991, **354**, 161–164.
5 J. Löwe and L. Amos, *Nature*, 1998, **391**, 203–206.
6 P. de Boer, *Current opinion in microbiology*, 2010, **13**, 730–737.
7 J. Lutkenhaus and S. Addinall, *Annual review of biochemistry*, 1997, **66**, 93–116.
8 D. Bramhill and C. Thompson, *Proc. Natl. Acad. Sci. USA*, 1994, **91**, 5813–5817.
9 H. Erickson, D. Taylor, K. Taylor and D. Bramhill, *Proc. Natl. Acad. Sci. USA*, 1996, **93**, 519–523.
10 A. Mukherjee and J. Lutkenhaus, *The EMBO Journal*, 1998, **17**, 462–469.
11 C. Lu and H. Erickson, *Cell Structure and Function*, 1999, **24**, 285–290.
12 P. Taschner, P. Huls, E. Pas and C. Woldringh, *Journal of bacteriology*, 1988, **170**, 1533–1540.
13 M. Osawa, D. Anderson and H. Erickson, *Science*, 2008, **320**, 792–794.
14 I. Surovtsev, J. Morgan and P. Lindahl, *PLoS computational biology*, 2008, **4**, e1000102.
15 Y. Chen and H. Erickson, *Journal of Biological Chemistry*, 2005, **280**, 22549–22554.
16 I. Hörger, E. Velasco, G. Mingorance, J. Rivas, P. Tarazona and M. Vélez,

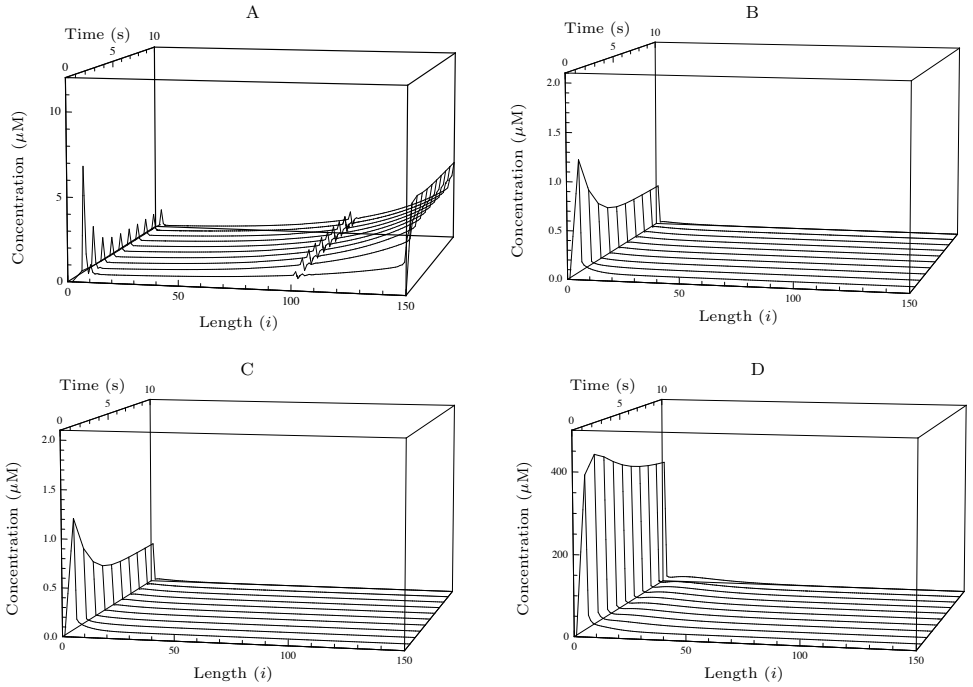

Fig. E 1 The effect of FtsZ diffusion between the cell caps and midcell compartments. FtsZ polymer concentrations are plotted for length i at different time points. Inclusion of FtsZ diffusion between the cell caps and the midcell region removes the accumulation of long open polymers seen in the Surovtsev model.[14] (A) The concentration of open FtsZ polymers in the "*in vivo*" Surovtsev model, $\xi = 0.001$, $\sigma = 0.5$, $k_{\mathrm{cyc1}} = 60\,\mathrm{s}^{-1}$, $k_{\mathrm{cyc2}} = 0.4\,\mathrm{s}^{-1}$. (B) The concentration of FtsZ polymers in the cell caps in the present model. (C) The concentration of FtsZ polymers in the midcell region in the present model. (D) The concentration of FtsZ polymers in the midcell membrane compartment in the present model. All parameter values as shown in Table 1.

Physical Review E: Statistical, Nonlinear, and Soft Matter Physics, 2008, **77**, 011902.

17 I. Hörger, E. Velasco, G. Rivas, M. Vélez and P. Tarazona, *Biophysical Journal: Biophysical Letters*, 2008, **94**, L81–L83.

18 D. Turner, I. Portman, T. Dafforn, A. Rodger, D. Roper, C. Smith and M. Turner, *Biophysical Journal*, 2012, **102**, 731–738.

19 I. Surovtsev, Z. Zhang, P. Lindahl and J. Morgan, *Journal of Theoretical Biology*, 2009, **260**, 422–429.

20 G. Lan, C. Wolgemuth and S. Sun, *Proc. Natl. Acad. Sci. USA*, 2007, **104**, 16110–16115.

21 W. Margolin, *Nature Reviews Molecular Cell Biology*, 2005, **6**, 862–871.

22 P. Mateos-Gil, A. Paez, I. Hörger, G. Rivas, M. Vicente, P. Tarazona and M. Vélez, *Proc. Natl. Acad. Sci. USA*, 2012, **109**, 8133–8138.

23 H. Erickson, *Proc. Natl. Acad. Sci. USA*, 2009, **106**, 9238–9243.

24 D. RayChaudhuri and J. T. Park, *Nature*, 1992, **359**, 251–254.

25 L. Romberg and T. Mitchison, *Biochemistry*, 2004, **43**, 282–288.

26 Y. Chen, K. Bjornson, S. Redick and H. Erickson, *Biophys. J.*, 2005, **88**, 505–514.

27 D. Scheffers, J. de Wit, T. den Blaauwen and A. Driessen, *Biochemistry*, 2002, **41**, 521–529.

28 D. Scheffers, J. de Wit, T. den Blaauwen and A. Driessen, *FEBS letters*, 2001, **494**, 34–37.

29 S. Pichoff and J. Lutkenhaus, *Molecular Microbiology*, 2005, **55**, 1722–1734.

30 Z. Liu, A. Mukherjee and J. Lutkenhaus, *Molecular Microbiology*, 1999, **31**, 1853–1861.

31 T. Beuria, S. Mullapudi, E. Mileykovskaya, M. Sadasivam, W. Dowhan and W. Margolin, *Journal of Biological Chemistry*, 2009, **284**, 14079–14086.

32 C. Lu, J. Stricker and H. Erickson, *Cell Motil Cytoskeleton*, 1998, **40**, 71–86.

33 S. Rueda, M. Vicente and J. Mingorance, *Journal of bacteriology*, 2003, **185**, 3344–3351.

34 J. Pla, M. Sánchez, P. Palacios, M. Vicente and M. Aldea, *Molecular Microbiology*, 1991, **5**, 1681–1686.

35 L. Romberg, M. Simon and H. Erickson, *J. Biol. Chem.*, 2001, **276**, 11743–11753.

36 C. Culbertson, S. Jacobson and J. Ramsey, *Talanta*, 2002, **56**, 365–373.

37 B. Corbin, Y. Wang, T. Beuria and W. Margolin, *Journal of Bacteriology*, 2007, **189**, 3026–3035.

38 K. Schmidt, N. Peterson, R. Kustusch, M. Wissel, B. Graham, G. Phillips and D. Weiss, *Journal of Bacteriology*, 2004, **186**, 785–793.

39 J. Stricker, P. Maddox, E. Salmon and H. Erickson, *Proc. Natl. Acad. Sci. USA*, 2002, **99**, 3171–3175.

40 S. Haney, E. Glasfeld, C. Hale, D. Keeney, Z. He and P. de Boer, *Journal of Biological Chemistry*, 2001, **276**, 11980–11987.

41 A. Martos, C. Alfonso, López-Navajas, R. Ahijado-Guzmán, J. Mingorance, A. Minton and G. Rivas, *Biochemistry*, 2010, **49**, 10780–10787.

42 A. Mukherjee, K. Dai and J. Lutkenhaus, *Proc. Natl. Acad. Sci. USA*, 1993, **90**, 1053–1057.

43 D. Anderson, F. Gueiros-Filho and H. Erikson, *Journal of Bacteriology*, 2004, **186**, 5775–5781.

44 C. Hale and P. De Boer, *Journal of Bacteriology*, 1999, **181**, 167–176.

45 M. Oliva, S. Cordell and J. Löwe, *Nature structural & molecular biology*, 2004, **11**, 1243–1250.

46 J. Mingorance, S. Rueda, P. Gómez Puertas, A. Valencia and M. Vicente,

Molecular Microbiology, 2001, **41**, 83–91.
47 Y. Chen and H. Erickson, *Biochemistry*, 2009, **48**, 6664–6673.
48 S. Huecas, C. Schaffner-Barbaero, W. García, H. Yébenes, J. Palacios, J. Díaz, M. Menédez and J. Andreu, *Journal of Biological Chemistry*, 2007, **282**, 37515–37528.
49 E. Small, R. Marrington, A. Rodger, D. Scott, K. Sloan, D. Roper, T. Dafforn and S. Addinall, *Journal of Molecular Biology*, 2007, **369**, 210–221.
50 R. Pacheco-Gómez, X. Cheng, M. Hicks, C. Smith, D. Roper, S. Addinall, A. Rodger and T. Dafforn, *Biochemical Journal*, 2013, **449**, 795–802.
51 Q. Sun and W. Margolin, *Journal of bacteriology*, 1998, **180**, 2050–2056.
52 T. Den Blaauwen, N. Buddelmeijer, M. Aarsman, C. Hameete and N. Nanninga, *Journal of bacteriology*, 1999, **181**, 5167–5175.
53 R. Astumian, *Science*, 1997, **276**, 917–922.
54 R. Astumian and I. Derenyi, *Eur. Biophys. J.*, 1998, **27**, 474–489.
55 A. Feucht, I. Lucet, M. Yudkin and J. Errington, *Molecular microbiology*, 2001, **40**, 115–125.